Results in Optics 12 (2023) 100443

Contents lists available at ScienceDirect

Results in Optics

journal homepage: www.sciencedirect.com/journal/results-in-optics

Negative group-delay assisted anomalous propagation in stacked Split Ring Resonator array☆

V.P. Sarin [a,*], Rohith K. Raj [b,1], Vasudevan Kesavath [c,1]

[a] Department of Electronics, Govt. College Chittur, Palakkad, Kerala, India
[b] Department of Electronics, Govt. College Mananthavady, Wayanad, Kerala, India
[c] CREMA Lab, Department of Electronics, Cochin University of Science and Technology, Kerala, India

ARTICLE INFO

Keywords:
Anomalous dispersion
Metasurface
Negative group delay
Spilt-Ring Resonators

ABSTRACT

This paper explores a novel method to achieve negative group delay-assisted anomalous propagation without significant signal attenuation using stacked Split-Ring Resonator (SRR) array in the microwave regime. A sub-wavelength stacking thickness between the SRR layers creates transverse magnetic dipole moments due to the excitation of anti-parallel currents on these layers resulting in increased transmission amplitude. Multipole scattering theory has been utilized to extract the reason behind anomalous propagation by evaluating the scattered power from the principal electric and magnetic dipole moments excited on the structure. Time-domain analysis are performed on the samples, and negative group delay behavior is confirmed by observing the precedence of the output electromagnetic Gaussian pulse within the anomalous dispersion regime. The coupling effects are studied numerically using full-wave solvers and verified in experiments by performing transmission measurements inside an anechoic chamber.

1. Introduction

According to Einstein's special theory of relativity, the speed of any moving particle cannot exceed light velocity *c*. When an electromagnetic pulse enters a linear dispersive medium characterized by a refractive index n(ω), it travels with a group velocity $V_g = c/n_g$, where n_g is the group index. If the group velocity remains constant over the spectrum, then the shape of the pulse is unaffected by the medium. In electromagnetically induced transparency (EIT) schemes, the group velocity is significantly reduced, resulting in a slow light phenomenon (Baraclough et al., 2018; Brillouin, 1946), and one could even stop light for applications related to optical storage. An important parameter that characterizes electromagnetic wave propagation is the phase characterization known as group delay (GD). This concept was proposed by Nyquist to characterize phase linearity or dispersion and is defined as

$$\tau_g = -\frac{d\Phi(\omega)}{d\omega} \tag{1}$$

where $\phi(\omega)$ is the transmission phase and ω is the angular frequency. This means that group delay is the negative slope of transmission phase; a negative slope gives a positive group delay (PGD) and a positive slope gives a negative group delay (NGD). Normally NGD is observed within the frequency ranges showing strong electromagnetic absorption and such a medium is said to be exhibiting anomalous dispersion in which the group velocity is greater than the phase velocity, v_c or it can be even negative (Brillouin, 1960; Chaudhary and Jeong, 2015).

The concept of electromagnetic wave propagation through an anomalous dispersion region of a Lorentzian medium was extensively studied by Sommerfeld and L. Brillouin in 1914 (Chu and Wong, 1982; Donzelli et al., 2009) followed by the work of Lord Rayleigh (Fleischhauer et al., 2005). Within the anomalous dispersion region, the group index $\partial Re(n)/\partial\omega$ will be negative, and the signal undergoes significant attenuation. In such a case, the Gaussian pulse is found to be advanced in time while traversing the medium or, alternatively, the output peak precedes the input. Before the work of Brillouin, the wave propagation through an anomalous dispersion region was considered to be superluminal, violating causality. However, Brillouin proposed a variety of wave velocities like phase, group, energy, front, and first/ second precursor velocities; among which the "front velocity" describes the

☆ This research work was performed at the Electronics Lab, Govt. College Chittur, Palakkad, Kerala.

* Corresponding author.
E-mail address: sarincrema@gmail.com (V.P. Sarin).

[1] These authors contributed equally to the work.

https://doi.org/10.1016/j.rio.2023.100443
Received 14 January 2023; Received in revised form 23 March 2023; Accepted 30 April 2023
Available online 2 May 2023

velocity at which the information travels, which is found to be luminal in an anomalous dispersion media.

Years later, in the 1970s, Garret et al. studied the same problem and concluded that abnormal or negative group velocities are physically realizable under certain conditions (Garrett and McCumber, 1970). However, their studies showed that even though the Gaussian pulse's shape is unaffected, the pulse's amplitude is significantly attenuated. The first experimental demonstration of abnormal propagation was performed by Chu et al. in 1982 in which a picosecond laser pulse is allowed to propagate through the absorption line of the GaP:N sample (Gupta et al., 2016). Anomalous propagation is also observed in under sized waveguides (Hesmer et al., 2007), misaligned horn antenna (Kandic and Bridges, 2011), and in side by side prisms (Mirzaei and Eleftheriades, 2013).

Anomalous dispersion media or equivalently NGD devices in the form of RLC resonators (Mitchell and Chiao, 1998) and bandstop filters (Mojahedi et al., 2000) are conventionally used to improve isolation characteristics by reducing reflections in the form of standing waves from the circuitry. NGD can also be implemented by using negative permittivity composites in which the negative slope of effective dielectric constant causes significant electromagnetic absorption resulting in an enhanced shielding efficiency (Mojahedi et al., 2000; Mojahedi et al., 2003). NGD devices are very useful for phase delay compensation caused due to PGD and hence could be used as time-delay compensators in sensor networks (Mugnai et al., 1998), eliminating phase variations in broadband phase shifters (Mumby and Yuan, 1989), and also in realizing non-Foster reactive elements (Pendry et al., 1999).

Recently, considerable research interest has been devoted to the development of Left-Handed Media (LHM). LHM consists of artificial inclusions of Split-Ring Resonators (SRR) and wire pair arrays to generate a negative index of refraction (Powell et al., 2011). The LHM supports positive and negative group velocities corresponding to the passband and stopband regions. Negative group velocity is achieved by satisfying the condition $\partial Re(n)/\partial\omega < 0$ in the anomalous propagation region of the LHM media. Eleftheriades and Mojahedi have studied the performance of an LHM media supporting anomalous dispersion in both the time and frequency domains analytically and experimentally (Ranfagni et al., 1991; Ranfagni et al., 1993; Ravelo et al., 2008; Rayleigh, 1899). The major disadvantage of media possessing abnormal propagation is that the transmitted signal is significantly attenuated within the narrow anomalous dispersion window.

In this paper, we propose the existence of negative group delay-assisted anomalous or abnormal wave propagation without significant signal attenuation using stacked SRR arrays having a subwavelength inter-array thickness in the microwave range. SRR array is a good choice to obtain negative permeability values around resonance (Smith et al., 2000) under the $H_{||}$ excitation scenario. Here we are using the $H_{\perp}$ excitation scenario and used two similar SRR arrays stacked with subwavelength thickness to yield an anomalous dispersion band with less signal attenuation. Experimental studies are performed inside an anechoic chamber using a vector network analyzer, and computations are performed using the full-wave electromagnetic simulation software CST Microwave Studio.

2. The geometry of the problem

The basic metasurface element used in the study is the Split Ring Resonator (SRR). In this study, we used the $H_{\perp}$ excitation and stacked two SRR unit cells along the propagation direction, as shown in Fig. 1. When an external plane wave with the electric field parallel to the splits along the Y-axis with the magnetic field parallel to its axis along the Z-axis is incident on the array, strong magnetic dipole moments will be excited. This excitation is referred known as the $H_{||}$ excitation (Powell et al., 2011). But in the $H_{\perp}$ excitation, the incident electric field is made parallel to the split (along Y-axis), the magnetic field is perpendicular to the axis of the SRR (along X-axis), and the direction of propagation is oriented along the axis of the SRR (along Z-axis).

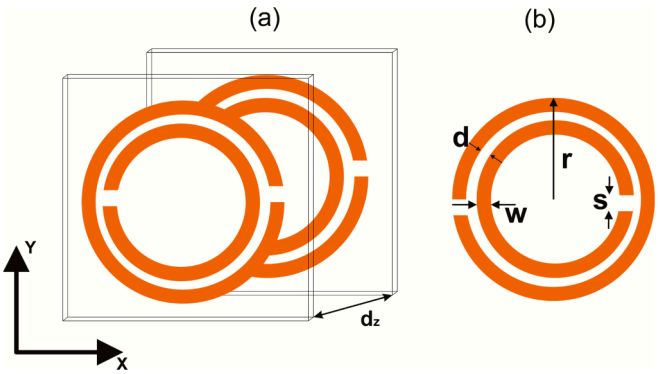

Fig. 1. Geometry of the stacked SRR uni cell.

The SRR array is printed on an epoxy substrate having a relative dielectric constant of 4.4 (Sreekala et al., 2020) and a height of 0.6 mm. The split gap is represented by 's'. The dimensions of the SRR are selected such that its resonant frequency lies within the microwave S-band. The stacking thickness is denoted as 'd_z' as shown in Fig. 1. Fig. 1 (b) describes the geometrical parameters of the SRR.

3. Unit cell simulation results

The concept of anomalous propagation in stacked SRR metasurface is computationally analyzed using the full-wave CST Microwave Studio software. The parameters of the proposed SRR array used for simulation are $r = 6.7$ mm, $d = 2$ mm, $s = 0.8$ mm, and $w = 1$ mm. The metallic structure is printed on a low-cost epoxy substrate having a relative dielectric constant $\varepsilon_r = 4.4$ and height h = 0.6 mm. The thickness of the Copper deposition is 35 μm and in simulations metal parts are treated as Perfect Electric Conductors (PEC). The periodicity of the SRR array is p = 20 mm along the X and Y directions. The stacking thickness is denoted by d_z and this parameter is optimized after parametric simulations. We have also simulated a single-layer SRR array having the same dimensions for a comparison study and this array contains 64 SRR elements in the plane. However, for simulations, we have simulated only the unit cell by applying the periodic boundary conditions along the X and Y axis of the unit cell shown in Fig. 1.

Fig. 2 illustrates the transmission magnitude and phase of the single and stacked SRR arrays under investigation. From Fig. 2 (a), it is clear that the single SRR array shows a highly reflective resonance around 2.3 GHz, as indicated by the solid blue line. The transmission coefficient at this resonance is found to be very low. This resonance is caused due to the excitation of electric dipole moments due to the oscillation of positive and negative charges on the top and bottom SRR cells. This is a highly scattering resonance and its quality factor is low. The metasurface scatters power equally along the azimuth plane, and hence an external observer can detect this resonance from the far-field. The transmission phase of this electric dipole resonance shows a smooth, positive transition around the resonant frequency as shown in Fig. 2(b).

When two SRR arrays are brought close together with subwavelength stacking thickness, there will be electric and magnetic coupling resulting in symmetric and anti-symmetric resonances (Steinberg and Chiao, 1994; Taher and Farrell, 2016; Wan et al., 2019). The symmetric resonance is caused due to the in-phase currents on the plates and the anti-symmetric resonance is excited due to the out-of phase current distributions on the stacked plates. It is interesting to note that stacking two layers of similar SRR as shown in Fig. 1 (a), predominantly modifies the transmission spectrum. This stacked array's transmission characteristics are indicated with solid red lines in Fig. 2. As expected, the stacked SRR shows two resonant dips, designated as I and II in the

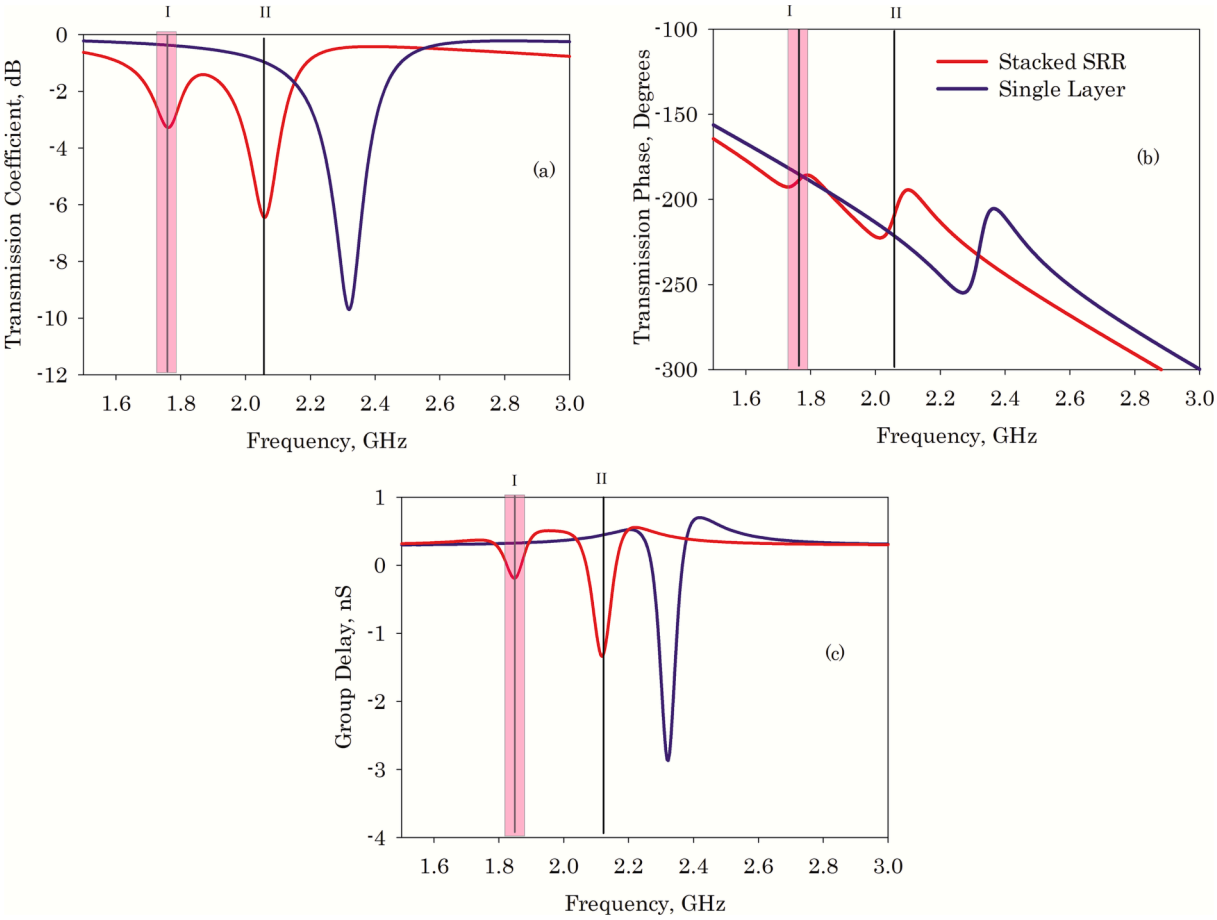

Fig. 2. Transmission response of the single SRR (solid blueline) and the stacked SRR (solid red line) arrays a) Transmission Coefficient, b) transmission phase and c) group delay. (For interpretation of the references to colour in this figure legend, the reader is referred to the web version of this article.)

diagram. Resonance II at 2.1 GHz, is designated as the symmetric resonance in which the currents on the stacked SRR are in-phase and shows a transmission coefficient of −6.5 dB. Resonance I found around 1.78 GHz is called as the anti-symmetric resonance of the stacked pair. The transmission coefficient is significantly higher as compared to the symmetric higher resonance and is of the order of −3.5 dB. The interesting behavior is that this resonance is accompanied by advancement in the transmission phase. Hence it is called as an anomalous transmission resonance accompanied by a large transmission coefficient. The anomalous dispersion region is indicated using the shaded region in the graph. The peculiarity of this resonance is that the group delay, which is related to the negative rate of change of transmission phase with frequency ($-d\Phi/d\omega$), will be negative as dictated in Fig. 2(c). The group delay is of the order of −0.2 ns. Usually, this happens near the absorption line of a Lorentzian dispersion medium and is accompanied by a significant amplitude loss of electromagnetic pulse. However, here, the advantage is that the anomalous resonance is accompanied by a high value of transmission coefficient without signal distortion.

4. Parametric analysis

Parametric analyses have been performed on the metasurface to find out the effect of stacking thickness d_z on transmission response. Fig. 3(a) and (b) show the effect of stacking thickness on transmission coefficient and transmission phase. The stacking parameter is varied from 0 mm to 0.4 mm in steps of 0.2 mm, and.

throughout the simulation, the thickness of both the substrates is kept constant at 0.6 mm. As the stacking thickness is increased, the anomalous resonance is blue-shifted, and it eventually merges with the second resonance from $d_z = 0.4mm$ onwards. For larger stacking thickness, the presence of an air layer between the two substrates reduces the effective dielectric constant causing a blue shift for the anomalous resonance and eventually it merges with the second resonance. Hence from $d_z = 0.4mm$ onwards a single resonance is observed which is said to be a merged resonance and this resonance is widely used to create electromagnetic wave absorbers in the microwave regime (Woodley and Mojahedi, 2004). The effect of variation in group delay against stacking thickness is shown in Fig. 3(c). It is clear that an increase in stacking thickness increases the magnitude of group delay and the merged resonance gives maximum group delay at the cost of reduced transmission magnitude.

We have also studied the effect of substrate thickness on the transmission characteristics of the metasurface and the results are illustrated in Fig. 4. In all these simulations, the relative permittivity of the sample is kept fixed at 4.4. As the substrate thickness is increased, the transmission dip for the lower anomalous resonant band is more visible and the transmission magnitude decreases. The increase in substrate thickness redshifts both the resonances and the magnitude of transmission coefficient is found to be increased for the higher resonance.

To find out the exact reason behind these peculiar transmission characteristics, the surface current and magnetic field distributions are studied for $d_z = 0.6mm$ and are depicted in Fig. 5. Fig. 5(a) and (b) represent the surface current and magnetic field distributions excited on the composite for a normal incident plane wave at 2.1 GHz. It is observed that the inner and outer rings of both the SRR are excited in-phase.

The in-phase excitation of both the lower and upper SRR creates strong H_z component of magnetic field directed axially along the center

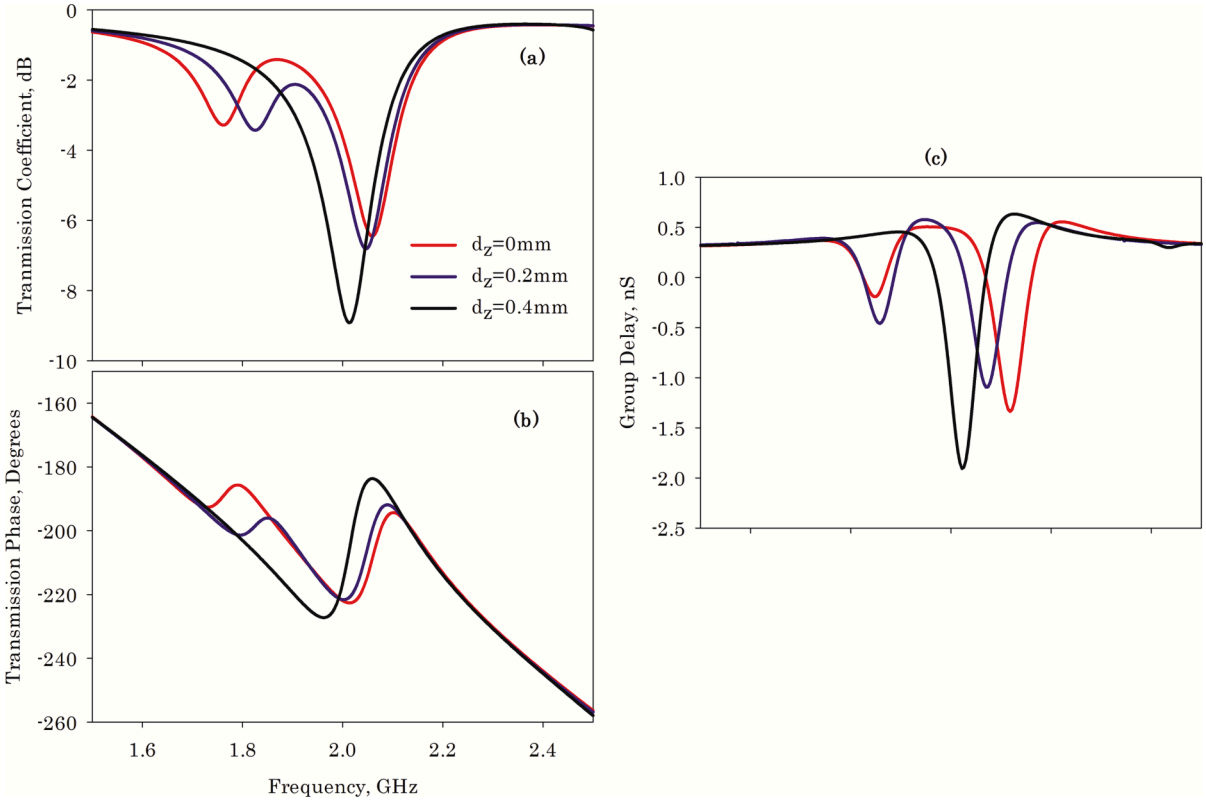

Fig. 3. Effect of stacking thickness d_z on a) transmission coefficient, b) transmission phase, and c) group delay.

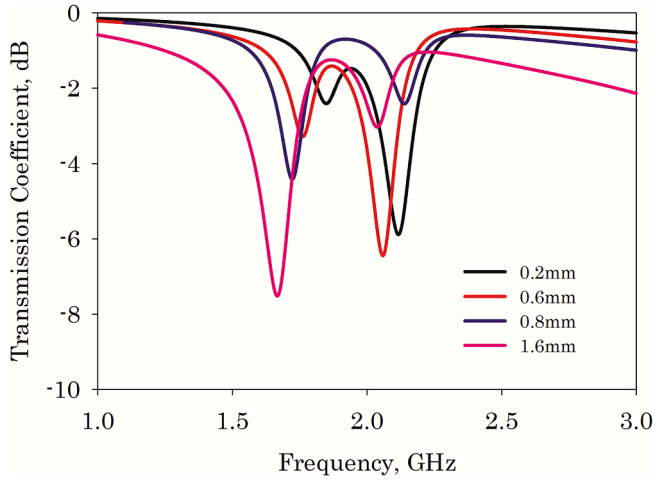

Fig. 4. Effect of substrate thickness transmission characteristics.

of the rings and hence the transmission for this resonance is prohibited causing a low transmission magnitude. Fig. 5 (c) and (d) represent the surface current and magnetic field distribution for the first resonance centered around 1.78 GHz respectively. It is evident that the outer rings of both the lower and upper SRR are excited and an anti-phase current distribution is observed on the stacked plates. This will create a transverse H_x component of the magnetic field. The H_x component of the magnetic field dominates over the H_z component causing transmission enhancement at this resonance.

5. Discussions with multipole theory

To clarify the reason behind this peculiar resonant behaviour, multipole scattering theory has been utilized. The multipolar decomposition provides an in-depth description of the scattering properties of the composite due to the induced charge-current distributions in which the scattered power from the induced multipoles could be calculated by integrating spatially distributed current distributions of the unit cell. The fundamental multipole amplitudes can be calculated as (Ravelo et al., 2008);

$$P = \frac{1}{i\omega}\int Jd^3r \tag{2}$$

$$M = \frac{1}{2c}\int (\vec{r}XJ)d^3r \tag{3}$$

where P is the electric dipole moment, M is the magnetic dipole moment, c is the velocity of light in vacuum, $\underset{r}{\rightarrow}$ is the displacement vector from the origin, ω is the angular frequency and J is the surface current density retrieved from simulations. The total power radiated from different multipole moments can be formulated as

$$I = \frac{2\omega^4}{3c^3}|P|^2 + \frac{2\omega^4}{3c^3}|M|^2 + \tag{4}$$

The normalized scattered power from the principal Electric Dipole (ED) and Magnetic Dipole (MD) for the single and stacked SRR arrays are illustrated in Fig. 6. From 6(a), it is evident that the single SRR array under $H_\perp$ excitation is characterized by the excitation of electric dipole moment at resonance and the contribution from the magnetic dipole is insignificantly small and hence can be neglected. For this excitation, the electric polarizability function is only slowly varying as pointed out by D.R Smith (Powell et al., 2011). It is obvious that anomalous resonance is caused due to the power scattering dip from the electric dipole resonance due to the destructive interference caused due to the out-of-phase oscillating surface currents on the stacked SRR layers. From Fig. 6(b), it is clear that the transmission enhancement for the anomalous resonance is caused by the excitation of magnetic dipole due to anti-symmetric

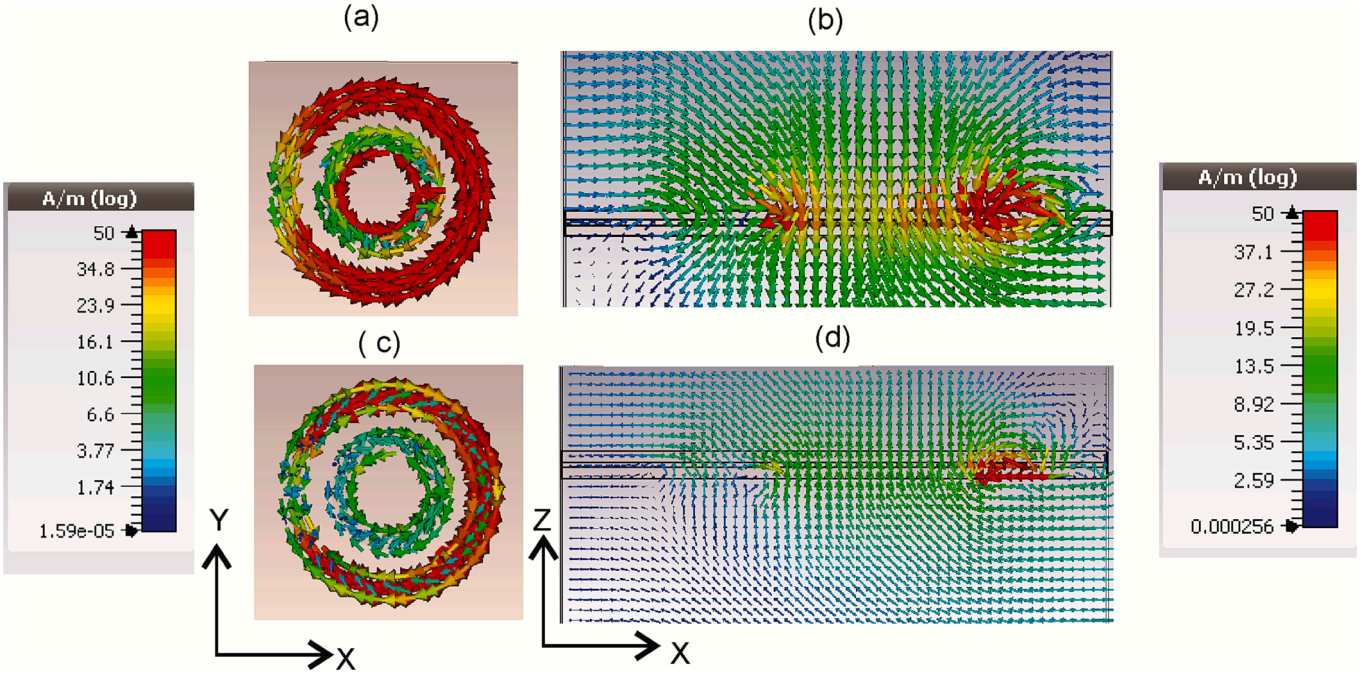

Fig. 5. Computed field distributions at resonances a) Surface current and b) Magnetic field distributions at 2.1 GHz, c) surface current and d) magnetic field distributions at 1.78 GHz.

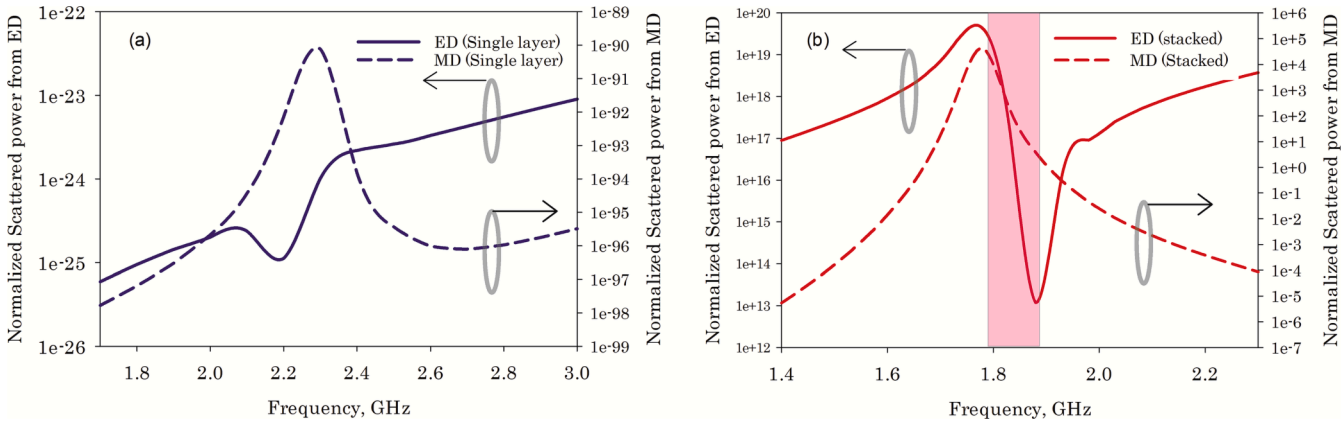

Fig. 6. Scattered power from principal multipoles for a) single layer SRR array and b) stacked SRR array.

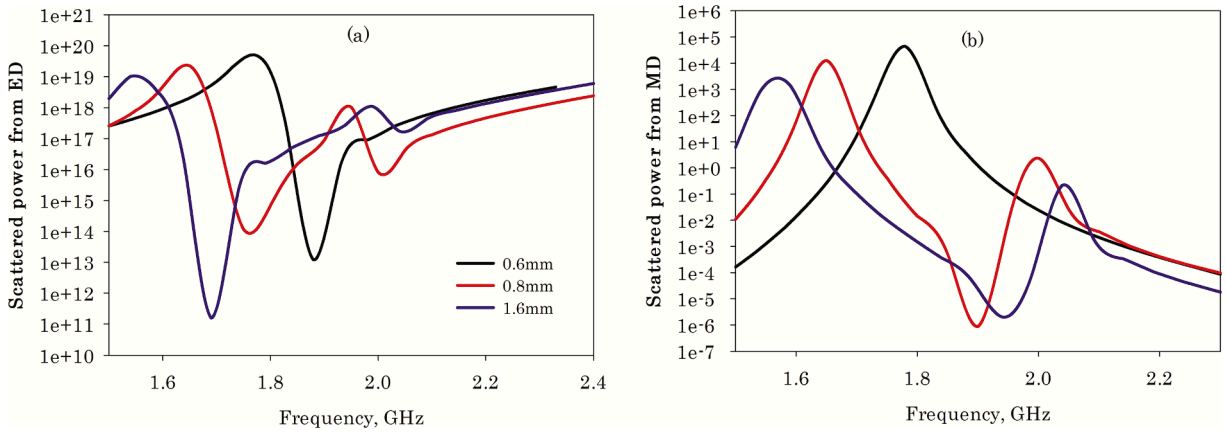

Fig. 7. Effect of variation in substrate thickness on scattered power a) scattered power from ED and b)scattered power from MD.

currents on the stacked SRR arrays. At the anomalous dispersion region, the power scattered from both ED and MD are decreasing with frequency. Even though the excitation of transverse magnetic dipole moment is weak in comparison with that of electric dipole moment, the negative slope of both these quantities causes absorption resulting in negative group delay.

We have also performed the effect of substrate thickness on scattered power and these results are illustrated in Fig. 7 for three different cases. It is observed that as the substrate thickness is increased, the coupling between the two SRR arrays decreases resulting in reduced scattered power from magnetic dipole as seen from Fig. 7(b). Since magnetic resonance is caused due to the coupling between two arrays, increase in substrate thickness effectively increases the resonant length through displacement current thereby decreasing the magnetic resonant frequency. As the substrate thickness is increased, transmitted power from the sample is found to be decreased and the resonant dip becomes more pronounced for the anomalous resonance. This is due to the fact that increase in substrate thickness reduces power scattered from the ED resonance and when the thickness is maintained at 1.6 mm, a more pronounced roll off is observed at resonance causing increased electromagnetic absorption resulting in an enhanced group delay at the cost of a low transmission magnitude. This resonance could be used for enhancing the shielding efficiency of anti-reflective coatings due to enhanced microwave absorption. As the substrate thickness is decreased, the magnitude of transmission coefficient is enhanced while maintaining the anomalous transmission phase advance and hence thin sheets of stacked SRR array can be used for adjusting phase response of a PGD spatial filter system. The advantage is that there is no need to implement a gain medium to compensate the signal attenuation offered by conventional anomalous dispersion media.

6. Time domain analysis

The effect of anomalous dispersion could be easily understood by studying the response of the metasurface in the time-domain. For that, a Gaussian sinusoidal signal is applied as the input signal of the plane wave in the full-wave simulations. Two probes are used to detect the input and output waveforms in the time domain. These probes are situated at a distance of 30 mm apart from the input and output faces of the metasurface and are used to detect the E_y component of electric field distribution. Time domain simulations are performed, and the recorded pulses are depicted in Fig. 8 for the anomalous propagation band around 1.78 GHz and for a normal plane wave propagation through the epoxy substrate at 1.8 GHz. It is observed from Fig. 6(a) that the peak of the output pulse precedes the input pulse by 2.15 ns. This pulse shift doesn't indicate that the Gaussian pulse travels at superluminal group velocities and this propagation scenario doesn't violate causality. The velocity of the traveling pulse is defined using the front velocity of the pulse, and here, it remains luminal. The pulse peak advancement is accounted due to the excessive phase shift offered by the anomalous dispersion medium resulting in a change in the shape of the pulse. It is seen that the amplitude of the propagating pulse is not significantly affected by the anomalous propagation medium. Fig. 6(b) depicts the transmission time response for a Gaussian plane wave through the epoxy substrate centered at 1.78 GHz. Here the pulse shape is unaffected by the dielectric layer, and a positive delay of 0.15 ns is observed between the input and output pulse peaks.

7. Measurement results

The metasurface samples are fabricated by adopting photolithographic techniques. The transmission coefficients are measured inside an anechoic chamber by configuring two Ultra Wideband horn antennas placed 1 m apart, as depicted in Fig. 9. Initially, a THRU calibration is performed in free space, and then the stacked metasurface is placed in between the horn antennas to record the transmission response.

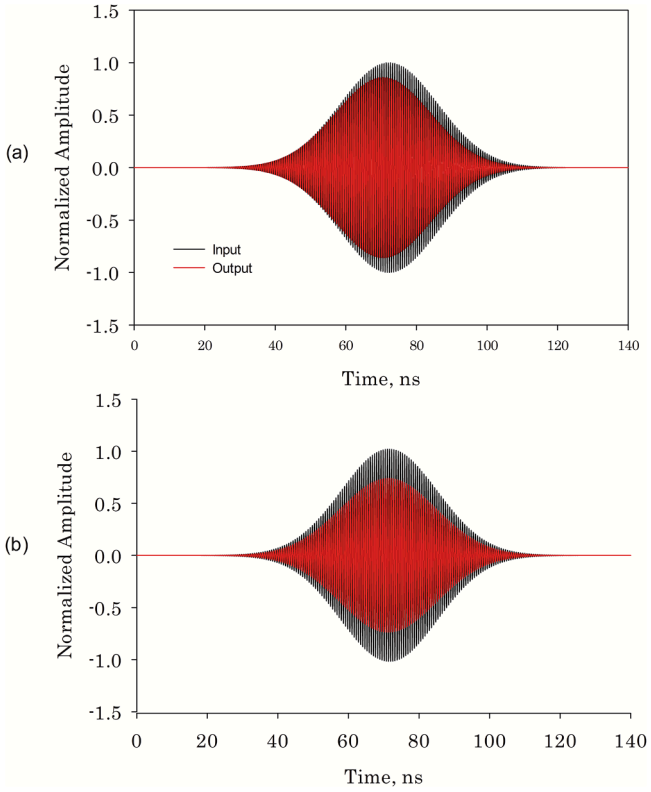

Fig. 8. Results of time-domain simulations using Gaussian sine waves a) for the anomalous dispersion band centered at 1.78 GHz and b) for a normal propagating plane wave in through the epoxy substrate in free space centered at 1.78 GHz.

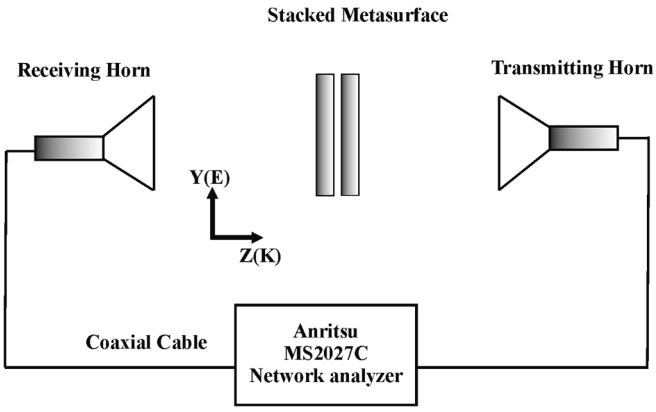

Fig. 9. Measurement setup to verify transmission response.

The transmission response of the fabricated metasurfaces is illustrated in Fig. 10. Fig. 10(a) shows the transmission response of the single SRR array. The resonant transmission dip is found to be around 2.34 GHz, and it shows a very low transmission coefficient of the order of −17.7 dB. Fig. 10(b) shows the transmission response of the stacked SRR metasurface with $d_z = 0mm$. The transmission response shows an excellent agreement with the simulation response. The electric dipole resonance is red shifted to 2.19 GHz (resonance II) due to the capacitive coupling between the stacked layers and shows a transmission coefficient value of −10 dB. The anomalous transmission band is around 1.75 GHz with a transmission magnitude of −4 dB designated as resonance I. The small mismatches are accounted due to the fabrication and measurement tolerences. The slope of the transmission phase around this resonance is found to be increasing. The measured group delay of the

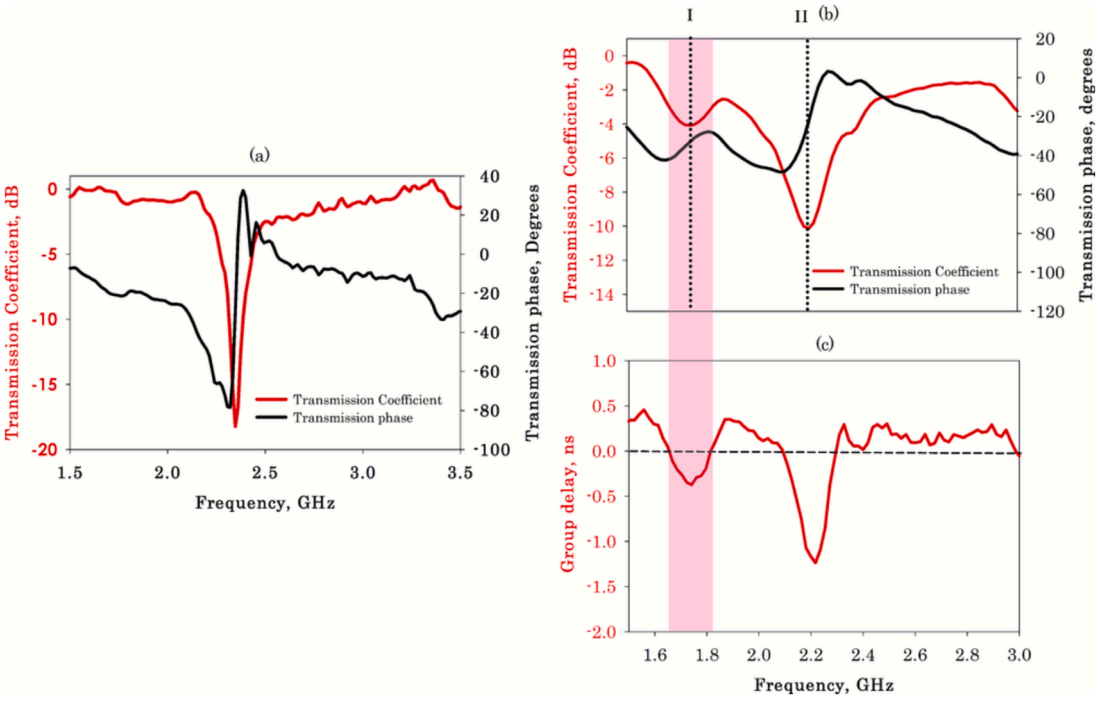

Fig. 10. Measurement results in the frequency-domain a) transmission response of single layer SRR array, b) transmission coefficient and phase of stacked SRR array and c) Group delay of the stacked SRR array.

stacked metasurface is shown in Fig. 10(c). Corresponding to the anomalous transmission resonance, the group delay is negative, thereby confirming the simulation results.

8. Conclusion

In this paper, we demonstrate the excitation of anomalous propagation without significant signal attenuation in a stacked Split-Ring Resonator metasurface operating in the microwave regime. The anomalous dispersion band is characterized by an increase in the transmission phase accompanied by a negative group delay. We have performed time-domain simulations, and it is found that anomalous dispersion results in the advancement of the Gaussian peak with respect to the input pulse peak. The simulation results are verified by measuring transmission coefficients inside an anechoic chamber in the frequency domain.

Data availability

Data will be available from the authors upon reasonable request.

Declaration of Competing Interest

The authors declare that they have no known competing financial interests or personal relationships that could have appeared to influence the work reported in this paper.

Data availability

Data will be made available on request.

Acknowledgment

The authors acknowledge the research funding received from the Science and Engineering Research Board (SERB), Department of Science and Technology, for the major research project ECR/2017/002204.

References

Baraclough, M., Hooper, I.R., Barnes, W.L., 2018. Investigation of the coupling between tunable split-ring resonators. Phys. Rev. B 98, 085146. https://doi.org/10.1103/PhysRevB.98.085146.
Brillouin, L., 1946. Wave Propagation in Periodic Structures. McGraw-Hill, New York.
Brillouin, L., 1960. Wave Propagation and Group Velocity. Academic, New York.
Chaudhary, G., Jeong, Y., 2015. Transmission-type negative group delay networks using coupled line doublet structure. IET Microw. Antennas Propag. 9 (8), 748–754. https://doi.org/10.1049/iet-map.2014.0351.
Chu, S., Wong, S., 1982. Linear pulse propagation in an absorbing medium. Phys. Rev. Lett. 48 (11), 738–741.
Donzelli, G., Vallecchi, A., Capolino, F., Schuchinsky, A., 2009. Metamaterial made of paired planar conductors: Particle resonances, phenomena and properties. Metamaterials 3, 10–27. https://doi.org/10.1016/j.metmat.2008.12.001.
Fleischhauer, M., Imamoglu, A., Marangos, J.P., 2005. Electromagnetically induced transparency: Optics in coherent media. Rev. Mod. Phys. 77 (2), 633–673.
Garrett, C.G.B., McCumber, D.E., 1970. Propagation of a Gaussian light pulse through an anomalous dispersion medium. Phys. Rev. A 1 (2), 305–313.
Gupta, M., Savinov, V., Ningning, X.u., Cong, L., Dayal, G., Wang, S., Zhang, W., Zheludev, N.I., Singh, R., 2016. Sharp toroidal resonances in planar terahertz metasurfaces, 201601611 Adv. Mater. 1–6. https://doi.org/10.1002/adma.201601611.
Hesmer, F., Tatartschuk, E., Zhuromskyy, O., Radkovskaya, A.A., Shamonin, M., Hao, T., Stevens, C.J., Faulkner, G., Edwards, D.J., Shamonina, E., 2007. Coupling mechanisms for split ring resonators: Theory and experiment. Phys. stat. sol. (b) 244 (4), 1170–1175. https://doi.org/10.1002/pssb.200674501.
Kandic, M., Bridges, G.E., 2011. Asymptotic limits of negative group delay in active resonator-based distributed circuits. IEEE Trans. Circuits Syst. 58 (8), 1727–1735. https://doi.org/10.1109/TCSI.2011.2107251.
Mirzaei, H., Eleftheriades, G.V., 2013. Realizing non-Foster reactive elements using negative group delay networks. IEEE Trans. Microw. Theory Techn. 61 (12), 4322–4332. https://doi.org/10.1109/TMTT.2013.2281967.
Mitchell, M.W., Chiao, R.Y., 1998. Causality and negative group delays in a simple bandpass amplifier. Am. J. Phys. 66, 14–19. https://doi.org/10.1119/1.18813.
Mojahedi, M., Schamiloglu, E., Hegeler, F., Malloy, K.J., 2000. Time-domain detection of superluminal group velocity for single microwave pulses. Phys. Rev. E 62 (4), 5758–5766.
Mojahedi, M., Schamiloglu, E., Agi, K., Malloy, K.J., 2000. Frequency-domain detection of superluminal group velocity in a distributed Bragg reflector. IEEE J. Quantum Electron. 36 (4), 418–424.
Mojahedi, M., Malloy, K.J., Eleftheriades, G.V., Woodley, J., Chiao, R.Y., 2003. Abnormal wave propagation in passive media. IEEE J. Selected Topics in Quantum Electron. 9 (1), pp. https://doi.org/10.1109/JSTQE.2002.807971.
Mugnai, D., Ranfagni, A., Ronchi, L., 1998. The question of tunneling time duration: a new experimental test at microwave scale. Phys. Lett. A 247 (4-5), 281–286.

Mumby, S., Yuan, J., 1989. Dielectric properties of FR4 laminates as a function of thickness and the electrical frequency of the measurement. J. Electron. Mater. 18 (2), 287–292. https://doi.org/10.1007/BF02657420.

Pendry, J.B., Holden, A.J., Robbins, D.J., Stewart, W.J., 1999. Magnetism from conductors and enhanced nonlinear phenomena. IEEE Trans. on Microw. Theory Tech. 47 (11), 2075–2084. https://doi.org/10.1109/22.798002.

Powell, D.A., Hannam, K., Shadrivov, I.V., Kivshar, Y.S., 2011. Near-field interaction of twisted split-ring resonators. Phys. Rev. B 83, 235420. https://doi.org/10.1103/PhysRevB.83.235420.

Ranfagni, A., Mugnai, D., Fabeni, P., Pazzi, G.P., 1991. Delay-time measurements in narrowed waveguides as a test of tunneling. Appl. Phys. Lett. 58 (7), 774–776.

Ranfagni, A., Fabeni, P., Pazzi, G.P., Mugnai, D., 1993. Anomalous pulse delay in microwave propagation: a plausible connection to the tunneling time. Phys. Rev. E 48 (2), 1453–1460.

Ravelo, B., Le Roy, M., Perennec, A., 2008. Application of negative group delay active circuits to the design of broadband and constant phase shifters. Microw. Opt. Technol. Lett. 50 (12), 3078–3080. https://doi.org/10.1002/mop.23883.

Rayleigh, L., 1899. The theory of anomalous dispersion. The London, Edinburgh, and Dublin Philosophical Magazine and Journal of Science 48 (290), 151–152. https://doi.org/10.1080/14786440608635663.

Smith, D.R., Padilla, W.J., Vier, D.C., Nemat-Nasser, S.C., Schultz, S., 2000. Composite Medium with Simultaneously Negative Permeability and Permittivity. Phys. Rev. Lett. 84 (18), 4184–4187.

Sreekala, P.S., John, Honey, Aanandan, C.K., 2020. Studies on anomalous dispersion behavior of PANI–CNT composites for enhanced shielding effectiveness in various microwave bands. Appl. Phys. A 126, 389. https://doi.org/10.1007/s00339-020-03583-6.

Steinberg, A.M., Chiao, R.Y., 1994. Dispersionless, highly superluminal propagation in a medium with a gain doublet. Phys. Rev. A 49, 2071–2075. https://doi.org/10.1103/PhysRevA.49.2071.

Taher, H., Farrell, R., "Highly miniaturized wideband negative group delay circuit using effective negative dielectric permittivity stopband microstrip lines," in Proc. 46th Eur. Microw. Conf., London, Oct. 4–6, , 112–115, 2016. doi: 10.1109/EuMC.2016.7824290.

Wan, F., Miao, X., Ravelo, B., Yuan, Q., Cheng, J., Ji, Q., Ge, J., 2019. Design of multi-scale negative group delay circuit for sensors signal time-delay cancellation. IEEE Sensors J. 19 (19), 8951–8962.

Woodley, J.F., Mojahedi, M., 2004. Negative group velocity and group delay in left-handed media. Phys. Rev. E 70, 046603. https://doi.org/10.1103/PhysRevE.70.046603.

Journal of Computational Electronics
https://doi.org/10.1007/s10825-022-01908-7

Demonstration of dipole-induced transparency using mirrored split-ring resonator metasurface for microwave applications

V. P. Sarin[1] · Rohith K. Raj[2] · Vasudevan Kesavath[3]

Received: 2 January 2022 / Accepted: 25 May 2022

Abstract
In this paper, the Dipole-Induced Transparency (DIT) in the microwave frequency regime is proposed and verified using experimental and simulation studies. A single-layer mirrored Split-Ring Resonator (SRR) array configured in the $H_{\perp}$ excitation scenario is used to create an out-of-phase oscillating electric dipole moment for a normal incident plane wave. The destructive interference between these out-of-phase oscillating electric dipole moments nullifies far-field scattering resulting in the emergence of the transparency window. We used the multipole scattering theory to validate the results computationally. The coupling effects are studied numerically, and the emergence of the transparency window is studied experimentally using transmission measurements inside an anechoic chamber using a vector network analyzer.

Keywords Dipole-induced transparency · Metasurface · Spilt-ring resonators

1 Introduction

Electromagnetically induced transparency (EIT) is a quantum interference effect occurring in atomic systems and is responsible for a transparency band within a broad absorption spectrum [1]. This transparency scheme modifies the dispersive nature of the opaque medium under consideration and shows electromagnetic wave slow down, resulting in enhanced light–matter interaction making the scheme suitable for electromagnetic sensing applications. EIT stems from the destructive interference from a multi-level system in which the net electric dipole moment of the atomic system is found to be vanished [2]. Under the EIT conditions, the propagating electromagnetic wave experiences a large positive dispersion, and its group velocity will be significantly reduced. This slow light effect is an essential characteristic of the EIT phenomenon and finds applications in quantum memories. When the light pulse enters an EIT medium, it gets slow down and undergoes spatial compression. The group velocity can be made zero by reducing the control field magnitude, causing the complete stopping of light and storing light within the medium [2].

EIT is also observed in classical coupled resonators in the optical domain [3], in resonator coupled optical waveguides [4], and in metamaterials [5–8]. In metamaterials, an external plane wave directly excites the bright resonance, which is efficiently coupled to the far field. The dark resonance is a high Q resonance and is weakly coupled to free space. An asymmetry in the unit cell creates resonant anti-parallel currents in the composite resulting in a trapped mode resonance [9–11]. The sharp dispersion associated with the trapped mode resonance causes the electromagnetic pulse to be significantly delayed of the order 200 times that of the velocity in free space.

The metasurface is a two-dimensional counterpart of metamaterials whose response is characterized using electric and magnetic polarizabilities and can be used for a wide range of applications [12, 13]. In this paper, we experimentally demonstrate the existence of Dipole-Induced Transparency in the microwave regime using a mirrored SRR metasurface. The emergence of the transmission band within the forbidden energy gap is characterized by the dip in the Radar Cross Section (RCS) of the composite. Multipole scattering theory reveals that the emergence of the transparency

✉ V. P. Sarin
sarincrema@gmail.com

[1] Department of Electronics, Govt. College Chittur, Chittur College PO, Palakkad, Kerala 678104, India

[2] Department of Electronics, Govt. College Mananthavady, Wayanad, Kerala 670645, India

[3] Centre for Research in Electromagnetics and Antennas, Department of Electronics, Cochin University of Science and Technology, Kochi, Kerala 682022, India

Published online: 20 June 2022

window is associated with scattering suppression due to the resonant out-of-phase oscillation of electric dipole moments excited on the composite. Experimental studies are performed inside an anechoic chamber using a vector network analyzer, and computations are performed using the full-wave electromagnetic simulation software CST Microwave Studio.

2 The geometry of the problem

The fundamental constituent used in the study is the Split-Ring Resonator (SRR). SRR unit cell is conventionally used to get the mu negative behavior at resonance [14]. The application of a plane wave with polarization parallel to the split with the incident magnetic field parallel to the axis of the SRR creates magnetic dipole moments parallel to the incident magnetic field. This excitation scenario is referred to as the $H_{||}$ excitation [15]. Another excitation is the $H_{\perp}$ scheme in which the incident electric field is parallel to the slits, the magnetic field is perpendicular to the axis of the SRR, and the direction of propagation is oriented along the axis of the SRR. This excitation creates strong electric dipole moments on the SRR array, and these in-phase oscillating electric dipole moments create a dielectric bandgap.

We have used the $H_{\perp}$ excitation in this study, and the difference is that the used SRR array is asymmetrical. We have used a mirrored array of SRR to create a transparency window within the dielectric bandgap as shown in Fig. 1. The SRR array is printed on an epoxy substrate having a relative dielectric constant of 3.8 and a height of 1.6 mm. The split gap is represented by 's.' The dimensions of the SRR are selected such that its resonant frequency lies within the microwave S-band. The offset parameter is represented as 'g' as shown in Fig. 1.

3 Results and discussions

The DIT behavior using the proposed mirrored configuration is computationally analyzed using the full-wave CST Microwave Studio software. The parameters of the proposed SRR array are $r = 6.7$ mm, $d = 2$ mm, $s = 0.8$ mm, $w = 1$ mm, and h = 1.6 mm. The thickness of the metallic implant is 35 µm. The periodicity of the SRR array is p = 20 mm mm both in

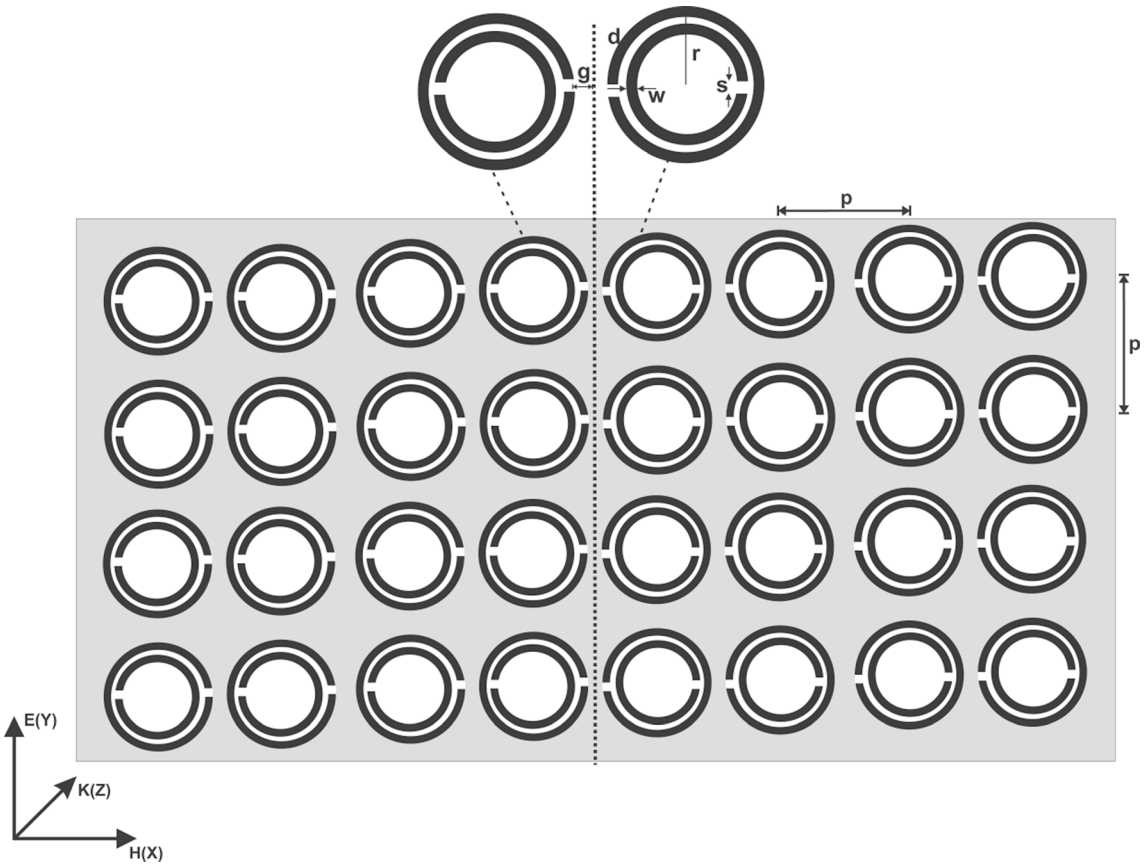

Fig. 1 Geometry of the mirrored SRR array

X and Y directions on both sides of the symmetry line. The asymmetry parameter 'g' is selected to be 1.1 mm. We have also simulated a single layer symmetric SRR array having the same dimensions and periodicity for a comparison study. Both the arrays use a total of 64 SRR elements in the plane. Both the arrays use a total of 64 SRR elements in the plane.

For simulations, both the structures are illuminated with a plane wave traveling perpendicular to the plane of the SRR array with polarization along the Y-axis. We have studied the scattering characteristics of both these arrays using computation. The Radar Cross Section (RCS) of a structure is defined as

$$\sigma = \lim_{R\to\infty} 4\pi R^2 \frac{|E_{sca}|^2}{|E_{inc}|^2} \quad (1)$$

where R is the distance from the target to the observation point, E_{inc} is the incident electric field measured at the target's position, and E_{sca} is the scattered electric field measured at the observation point. Figure 2 shows the RCS of the symmetric and mirrored SRR arrays. As expected, the symmetric SRR array shows a hike in the scattering spectra at resonance centered on 2.28 GHz. This resonance is characterized by the dominant scattering contribution from the electric dipole (P_y) moments. The RCS value is significantly higher of the order of around 30,425 mm^2 due to this bright electric dipole scattering and is said to be a highly visible resonance.

Interestingly, the RCS of the mirrored array shows low values indicated by the shadow region in comparison with the symmetric SRR array. The scattering reduction region spans over a frequency range from 2.16 GHz to 2.26 GHz. This mirrored array is characterized by two resonant peaks separated by a scattering dip. The scattering dip is observed at 2.17 GHz, and correspondingly, the RCS value is found to be 16,074 mm^2. The lower scattering hike is observed at 2.13 GHz with an RCS value of 18,336 mm2. The second scattering peak occurs at 2.29 GHz with an RCS of 31,634 mm^2.

Measurements are performed inside an anechoic chamber using two Ultra-Wide Band horn antennas. One horn antenna is configured in the transmission mode, and the other one is working in the reception mode. Initially, a THRU calibration is performed to nullify the path loss. The metasurface sample is inserted between these antennas to achieve the $H_{\perp}$ excitation scenario. The schematic of the measurement setup is shown in Fig. 3a. The resulting transmission coefficients for the symmetric SRR array are illustrated in Fig. 3b. As expected, the symmetric array shows a dielectric band gap centered around the resonant frequency $f_s = 2.28$ GHz, and correspondingly, the transmission coefficient is characterized by a dip showing resonant nature. The simulation and measurement are well matched. This resonance is characterized by strong electric dipole moments P_y and is caused due to the time-varying positive and negative charge distributions on the lower and upper unit cells. In the array, these electric dipole moments are oscillating in-phase, as shown in Fig. 3c. The scattering behavior of this SRR array is also studied by exciting the entire array with an external plane wave with polarization along the Y-axis using CST Microwave Studio. At resonance, the structure shows symmetric

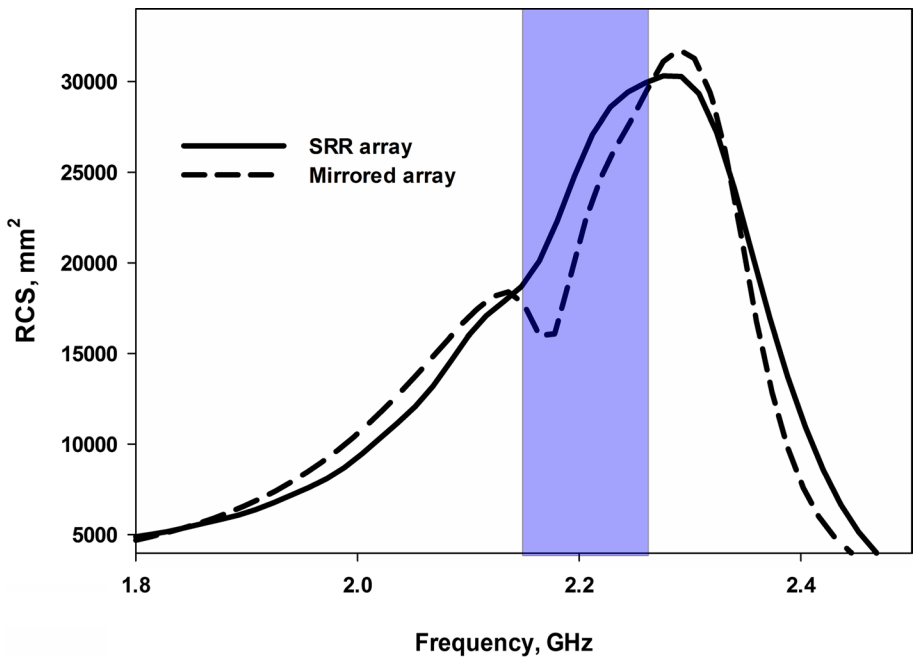

Fig. 2 RCS of the symmetric SRR array (solid line) and the mirrored array (dashed line)

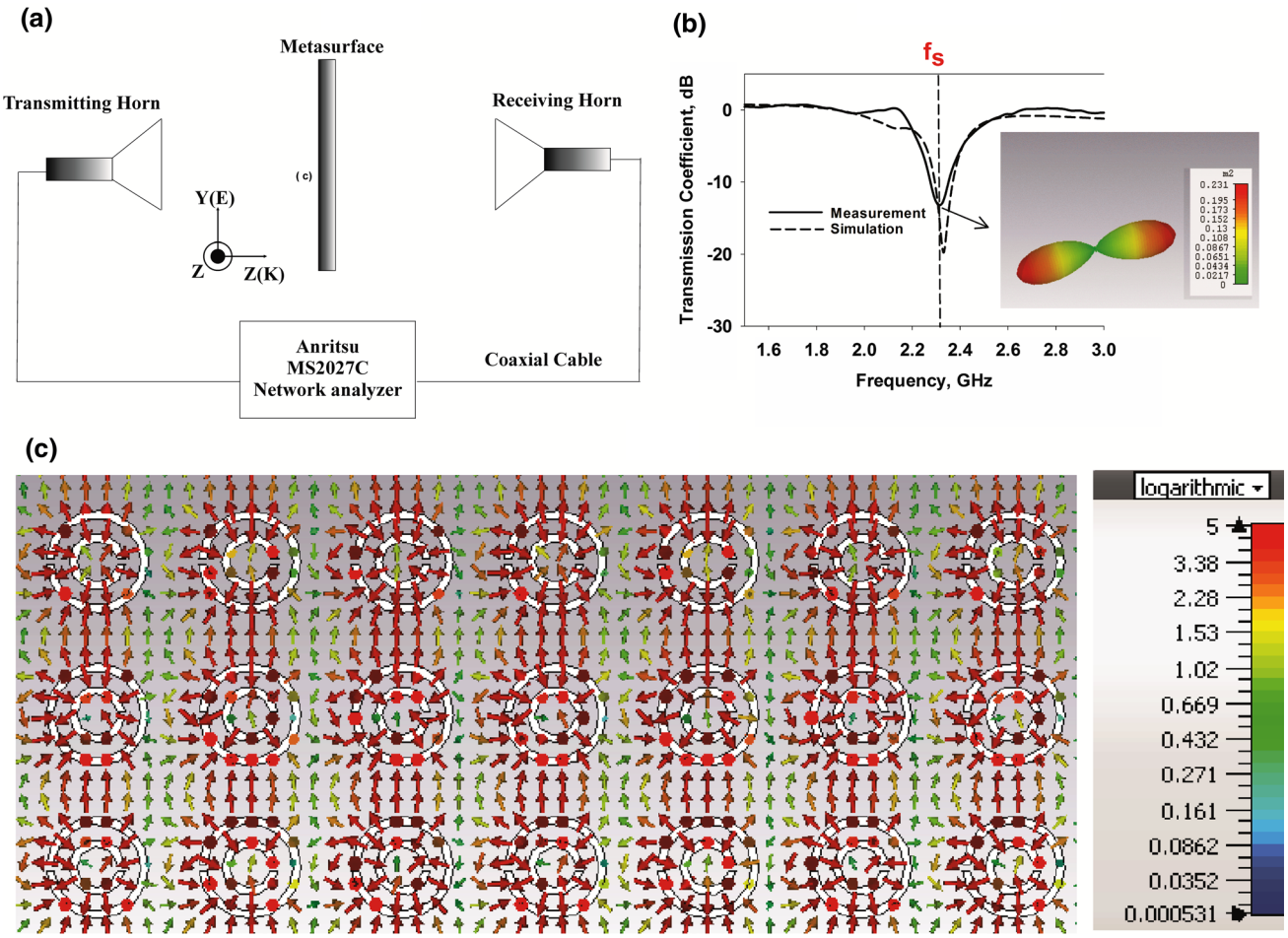

Fig. 3 **a** Measurement setup for characterizing the metasurface, **b** simulated and measured transmission coefficients of the SRR array, **c** electric field distribution at resonance (2.28 GHz)

forward and backward scattering, as shown in the inset of Fig. 3b.

The symmetric array showing the bandgap is replaced with the mirrored array configuration shown in Fig. 1. Figure 4 illustrates the transmission characteristics of this array. It is evident from the graph that a resonant transparency window is created within the bandgap for the mirrored array. This window is indicated using the shaded regions in the graph. Three resonant frequency points are observed designated as f_1, f_2, and f_3. The newly created resonant window is centered at $f_2 = 2.21$ GHz. The transmission coefficient at this transparency window is found to be -0.6 dB in measurement. The transmission minima are found to be at $f_1 = 2.13$ GHz and $f_3 = 2.32$ GHz. The simulation and measurements are well matched.

The measured transmission phase of the two arrays is depicted in Fig. 4b. The transmission phase shows distinctly different characteristics for the small frequency band under study. The symmetric SRR array shows smooth phase advancement across the bandgap. For the lower resonant dip around f_1, anomalous phase advancement is observed. Since the group delay is calculated as the negative rate of change of phase with frequency $\left(\tau = -\frac{d\Phi}{d\omega}\right)$, this region is characterized by a negative group delay (GD). So this resonant dip can be said as a trapped mode, in which the electromagnetic energy is strongly confined within the vicinity of the metasurface. The transparency band centered on f_2 shows a sharp decrease in phase with respect to frequency. Correspondingly, the group delay will be positive, causing a significant delay for the transmitted pulse. The reflection resonance at f_3 is characterized by an abrupt phase jump characterizing a reflective resonance. Since the transparency window is associated with a high group delay, the group velocity of the electromagnetic wave gets reduced. This ensures an enhanced light-matter interaction favorable for dielectric sensing applications. An unknown dielectric material inserted at the symmetry plane will shift the transparency peak to lower frequencies. So this technique could be used as a far-field sensor, in which Monostatic scattering

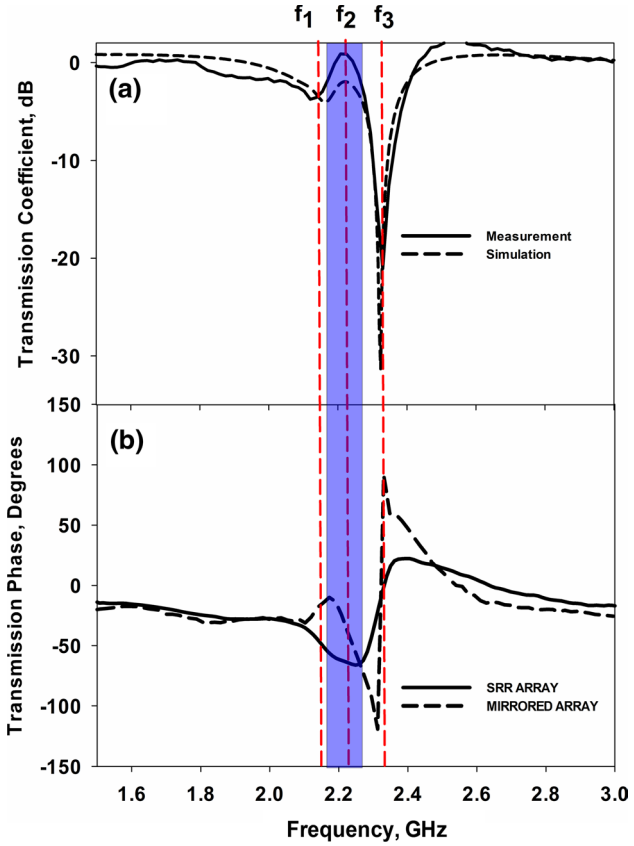

Fig. 4 **a** Simulated and measured transmission coefficients of the mirrored SRR array, **b** measured transmission phase of the mirrored and SRR arrays

measurements are enough to detect the unknown permittivity of the sample. Since electromagnetic waves around the transparency window are associated with a larger lifetime, the electromagnetic interaction with the sample is enhanced, resulting in a higher sensitivity.

Simulation studies are also performed to find out the nature of electromagnetic power flow across the dispersion band under consideration. Figure 5 shows the Poynting vector distributions of the mirrored array for the three frequency points. The plane wave is traveling along the Z-axis from top to the bottom of the computational domain. Obviously, for the trapped mode resonance centered around 2.16 GHz (Fig. 5a), a transverse flow of electromagnetic power is observed at the discontinuous boundary of the metasurface layer. The circulation of Poynting vector distribution near the metasurface boundary confirms the presence of the trapped mode. At this trapped mode resonance, the electromagnetic waves experience a large lifetime enabling maximum light–matter interaction. For the transparency window centered around 2.21 GHz (Fig. 5b), the pointing vector distributions are normal to the entrance and exit faces indicating a smooth electromagnetic power flow across the boundary. At this transparency window, the structure shows minimum scattering and is responsible for the RCS dip. This smooth flow of electromagnetic power is similar to that observed in electromagnetic cloaking schemes [16]. The highly reflective resonance shown in Fig. 5a around 2.32 GHz shows a significant perturbation of electromagnetic power flow and shows a high RCS value. It is noted that for the three frequency points, edge diffraction is observed on the left and right boundaries of the metasurface.

The scattering behavior of the mirrored array depicted in Fig. 2a shows a close similarity with a Fano resonance profile [17]. In Fano resonance, the destructive interference is achieved by the combined effect of electric and magnetic resonance to reduce total scattering and show asymmetric scattering profile. However, here the situation is quite different. We used the multipole scattering theory to understand the exact reason behind these peculiar scattering characteristics. Since the $H_{\perp}$ excitation scheme induces only the electric dipole moment on the SRR composite, only the power scattered from the electric dipole moment is expected. The induced dipole moments could be calculated by spatial integrating the surface current density excited on the composite as [18]

$$P = \frac{1}{i\omega} \int J \mathrm{d}^3 r \tag{2}$$

$$M = \frac{1}{2c} \int (\vec{r} X J) d^3 r \tag{3}$$

$$T = \frac{1}{10c} \int [(\vec{r}.J) - 2r^2 J] d^3 r \tag{4}$$

where P, M, T and represent the induced electric, magnetic, and toroidal dipole moments, ω is the angular frequency, J is the volume current density, r is the distance to the far-field observation point.

The normalized scattered power from these dipole moments for the symmetric SRR array is shown in Fig. 6. It is noted that the power radiated from the electric and toroidal dipole moments shows a dip around the transparency window. The radiated power from the electric dipole moment is less than that of the symmetric SRR array for the entire transparency window. For the symmetric array, the $H_{\perp}$ excitation scheme causes the separation of resonant positive and negative charges on the top and bottom SRR elements creating a net electric dipole moment (P_y) on the composite. Hence, this resonance is highly reflective, causing a transmission dip and a hike in RCS value around resonance. The mirrored configuration disturbs the uniform phase distribution of this excited electric dipole moment causing destructive interference at the far field. It is to be noted that the power radiated from the toroidal moment for

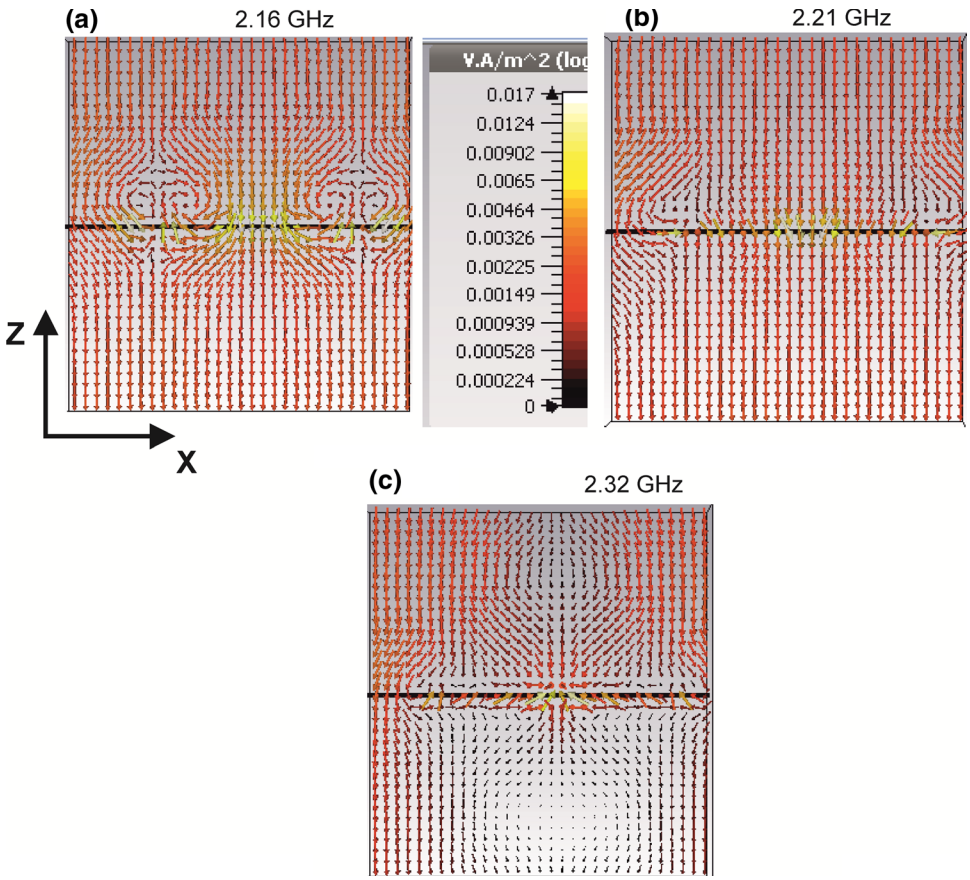

Fig. 5 Simulated Poynting vector distributions a) at 2.16 GHz, b) 2.21 GHz, and c) 2.32 GHz

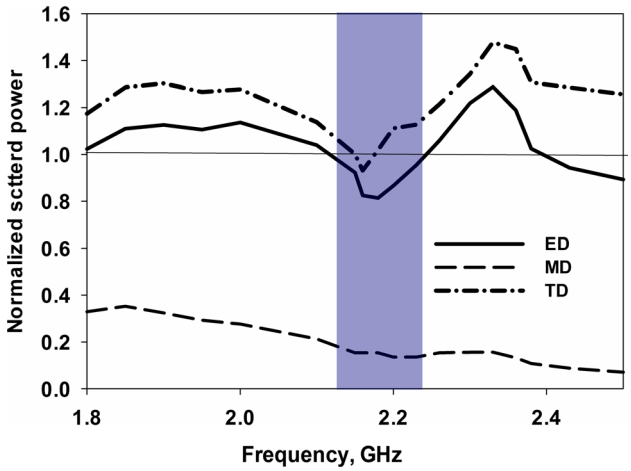

Fig. 6 Normalized scattered power from different multipoles

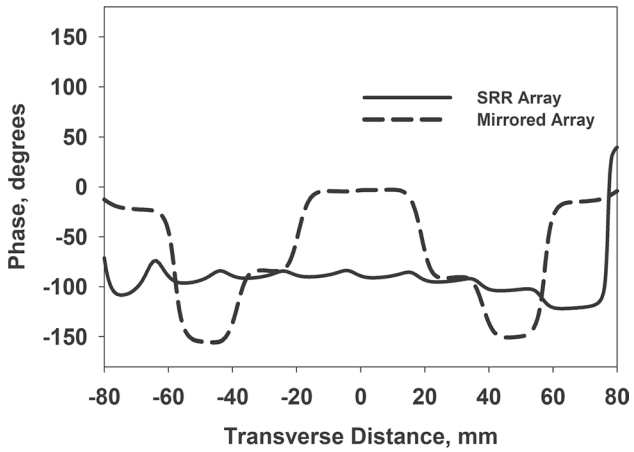

Fig. 7 Phase variation in electric field (Ey) distributions just above the two arrays

the mirrored array is in comparison with that for the mirrored array. Moreover, the electric dipole moment's radiated power is tremendously higher than that from the toroidal moment for the mirrored array. The magnetic dipole moment is non-resonant because the $H_{\perp}$ excitation scenario is incapable of exciting resonant magnetic dipole on the composite. The orientation of the magnetic dipole moment is directed along the direction of propagation (Z-axis), and hence, it is weekly coupled to free space. Hence, it can be concluded that the transparency window emerges due to the cancellation of radiated power from the electric dipole moment.

This scattering cancellation effect can be well understood by studying the phase of electric field distributions (E_y) taken over the two arrays, as shown in Fig. 7. It is observed

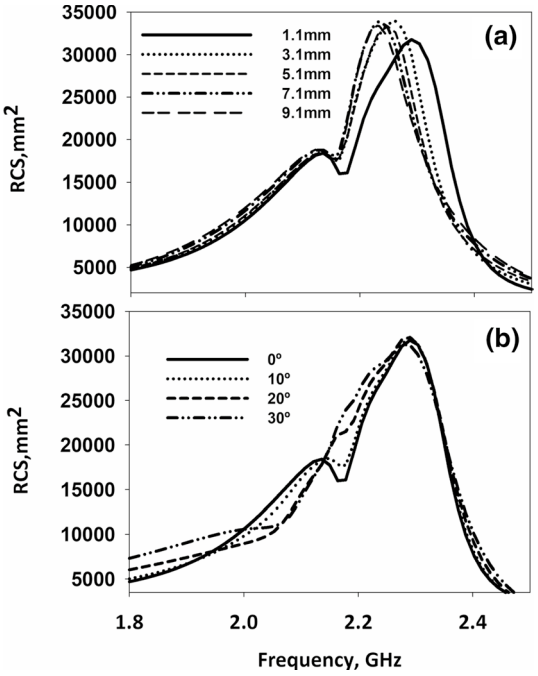

Fig. 8 Parametric variation studies **a** effect of gap parameter 'g' and **b** effect of angle of incidence in the azimuth plane on scattering characteristics

that for the symmetric array indicated by the solid black lines, the phase of the electric field across the array remains almost steady. It means that the electric dipole moments are oscillating in-phase resulting in a bandgap. However, the distributions show phase alterations around the symmetry line for the mirrored array as indicated by the black dashed lines. It is observed that the mirror SRR lying near the symmetry line are excited in-phase, whereas the distant ones are oscillating out-of-phase with respect to the center ones. These out-of-phase oscillations between the electric dipole moments cancel the far-field scattered power resulting in the emergence of the transparency window. An equivalent behavior is observed in the cloaking of a sensor or a metallic target [19, 20]. In this scenario, the far-field scattering offered by the electric dipole moment of the dipole or the sensor is cancelled by the out-of-phase scattering of the cloaking layer, and hence, the antenna is invisible to a far-field observer without deteriorating the radiation characteristics of the antenna. In the mantle cloaking technique, the electric surface reactance of the cloaking layer is adjusted to cancel the far-field scattering offered by the cloaking layer [21, 22].

Parametric analysis has been performed to find out the effect of various parameters on scattering spectra. Figure 8a shows the effect of the gap parameter 'g' on the scattering spectrum. For all these variations, a normal incidence plane wave is considered. It is observed that the scattering dip will be more pronounced when the mirrored elements are brought closer to each other. As 'g' is increased, a redshift in the scattering maximum is observed. When 'g' is increased above 3.1 mm, no significant change in the scattering dip is observed. Parametric studies have also been performed by varying the angle of incidence along the azimuth plane, and these results are shown in Fig. 8b. It is noted that the angle of incidence plays a crucial role on the scattering characteristics. The scattering dip around 2.17 GHz is clearly observed for normal incidence. As the angle of incidence increases in steps of 10°, the structure loses the scattering reduction behavior. When the incident angle is increased beyond 20°, the scattering behavior looks similar to the symmetric SRR array, and the transparency window is found to have vanished.

4 Conclusion

This paper presents an experimental and computational demonstration of Dipole-Induced Transparency scheme in the microwave regime. Multipole scattering theory has been utilized to find the exact reason behind the emergence of this transparency window. The mirror symmetry in the orientation of the SRR array creates an out-of-phase oscillation of electric dipole moments, resulting in scattering suppression from the composite at the far field. This scattering cancellation scheme is computationally verified using full-wave simulations and found that the transparency window is associated with a dip in the Radar Cross Section of the composite. Parametric studies have also been performed to find out the effect of various parameters on scattering characteristics. The high group delay associated with the transparency window will pave the way for developing an efficient far-field dielectric sensor in the future.

Acknowledgements The authors acknowledge the research funding received from the Science and Engineering Research Board (SERB), Department of Science and Technology, for the major research project ECR/2017/002204.

Funding The authors acknowledge the research funding received from the Science and Engineering Research Board (SERB), Department of Science and Technology, for the major research project ECR/2017/002204.

Data availability Enquiries about data availability should be directed to the authors.

Declarations

Conflicts of interest There are no conflicts of interest.

References

1. Xu, Q., Sandhu, S., Povinelli, M.L., Shakya, J., Fan, S., Lipson, M.: Experimental realization of an on-chip all-optical analogue to electromagnetically induced transparency. Phys. Rev. Lett. **96**(12) (2006)
2. Fleischhauer, M., Imamoglu, A., Marangos, J.P.: Electromagnetically induced transparency: optics in coherent media. Rev. Mod. Phys. **77**, 633 (2005)
3. Bajcsy, M., Zibrov, A.S., Lukin, M.D.: Stationary pulses of light in an atomic medium. Nature **426**(6967), 638–641 (2003)
4. Waks, E., Vuckovic, J.: Dipole induced transparency in drop-filter cavity-waveguide systems. Phys. Rev. Lett. **86**(15) (2006)
5. Dong, Z.-G., Liu, H., Cao, J.-X., Li, T., Wang, S.-M., Zhu, S.-N., Zhang, X.: Enhanced sensing performance by the plasmonic analog of electromagnetically induced transparency in active metamaterials. Appl. Phys. Lett. **97**(11) (2010)
6. Chakrabarti, S., Ramakrishna, S.A., Wanare, H.: Coherently controlling etamaterials. Opt. Exp. **16**(24), 19504–19511 (2008)
7. Liu, N., Langguth, L., Weiss, T., Kastel, J., Fleischhauer, M., Pfau, T., Giessen, H.: Plasmonic analogue of electromagnetically induced transparency at the Drude damping limit. Nature Mater. **8**(9), 758–762 (2009)
8. Kim, J., Soref, R., Buchwald, W.R.: Multi-peak electromagnetically induced ransparency (EIT)-like transmission from bull's-eye shaped metamaterial. Opt. Lett. **19**(17), 17997–18002 (2010)
9. Fedotov, V.A., Rose, M., Prosvirnin, S.L., Papasimakis, N., Zheludev, N.I.: Sharp trapped-mode resonances in planar metamaterials with a broken structural symmetry. Phys. Rev. Lett. **99**, 147401 (2007)
10. Chiam, S.-Y., Singh, R., Rockstuhl, C., Lederer, F., Zhang, W., Bettiol, A.A.: Analogue of electromagnetically induced transparency in a terahertz metamaterial. Phys. Rev. B **80**, 153103 (2009)
11. Papasimakis, N., Fedotov, V.A., Zheludev, N.I., Prosvirnin, S.L.: Metamaterial analog of electromagnetically induced transparency. Phys. Rev. Lett. **101**, 253903 (2008)
12. Bukhari, S.S., Vardaxoglou, J.Y., Whittow, W.: A metasurfaces review: definitions and applications. Appl. Sci. **9**(13), 2727 (2019)
13. Malik, J., Patnaik, A., Kartikeyan, M.V.: Modulated metasurface for circular polarization. In: Proceedings of the Asia-Pacific Microwave Conference (2016)
14. Pendry, J.B., Holden, A.J., Robbins, D.J.: Magnetism from conductors and enhanced nonlinear phenomena". IEEE Trans. Microwave Theory Techn. **47**(11), 2075–2084 (1999)
15. Smith, D.R., Padilla, W.J., Vier, D.C., Nemat-Nasser, S.C., Schultz, S.: Composite medium with simultaneously negative permeability and permittivity. Phys. Rev. Lett. **84**(18), 4184 (2000)
16. Alù, A., Engheta, N.: Cloaking a sensor. Phys. Rev. Lett. **102**, 233901 (2009)
17. Shafiei, F., Monticone, F., Le, K.Q., Liu, X.X., Hartsfield, T., Alù, A., Li, X.: A subwavelength plasmonic metamolecule exhibiting magnetic-based optical Fano resonance. Nature Nanotechnol. **8**(2), 95–99 (2013)
18. Papasimakis, N., Fedotov, V.A., Savinov, V., Raybould, T.A., Zheludev, N.I.: Electromagnetic toroidal excitations in matter and free space. Nat. Mater. **15**(3), 263–271 (2016)
19. Chachayma-Farfan, D.J., Radi, Y., Alù, A.: Dual-layer radiotransparent dielectric core metasurface antenna. IEEE Open J. Antennas Propag. **2**, 585–590 (2021)
20. Edwards, B., Alù, A., Silveirinha, M.G., Engheta, N.: Experimental verification of plasmonic cloaking at microwave frequencies with metamaterials. Phys. Rev. Lett. **103**(15), 153901 (2009)
21. Rizza, C., Matekovits, L.: Numerical investigation on graphene based mantle cloaking of a PEC cylinder. IEEE International Symposium on Antennas and Propagation and USNC-URSI Radio Science Meeting (2019)
22. Hamzavi-Zarghani, Z., Yahaghi, A., Matekovits, L.: Electrically tunable mantle cloaking utilizing graphene metasurface for oblique incidence. AEU Int. J. Electron. Commun. **116**, 153080 (2020)

ISSN: 2395-1680 (ONLINE)
DOI: 10.21917/ijme.2022.0228

CPW FED ULTRA COMPACT RADIATOR FOR 2.4 GHZ WIRELESS AND ISM APPLICATIONS

Sreejith M. Nair[1], Manju Abraham[2] and S. Sindhu[3]
[1,3]*Department of Electronics, Government College Chittur, India*
[2]*Department of Electronics, Baseliose Poulose II Catholicose College, India*

Abstract

A Uniplanar CPW fed electrically small radiator suitable for WiFi 802.11b, 802.11g, 802.11n, Bluetooth, ZigBee IEEE802.15.4 and ISM application is developed and presented. Physical structure of the developed antenna is very compact of the order of $0.12\lambda g \times 0.10\lambda g \times 0.02\lambda g$ which makes it very suitable for almost all the 2.4GHz based wireless applications. Parametric studies of the antenna is performed and from the results obtained design equations of the structure is developed and verified. Computational model of the antenna is also developed using FDTD and the results are compared and discussed. Antenna offers uniform radiation characteristics with good radiation efficiency and gain.

Keywords:

CPW Fed, Electrically Small, Short Based, Uniplanar

1. INTRODUCTION

Antenna plays a major and prime role in communication systems just like the sense organs in human beings, because they are used to perceive data from external world. As the size of communication gadgets decreases, it will create very interesting and complicated problems to antenna designers, so that they can design the compact antennas very first. The size reduction of antenna should not compromise its performance such as radiation pattern, gain efficiency etc too. Different techniques through which compactness can be achieved is discussed in various literatures.

A compact antenna suitable for 2.4GHz WLAM application is presented in [1] whose radiating element consists of a semicircular slot and an arc-shaped slot which are placed very near to the feed point. A reflector-based antenna which operates in two bands is presented in [2] which is huge when compared to our design. A pattern reconfigurable antenna based on PIN diodes is presented in [3] which comprises of complex structural specifications.

Yadav and Baudha [4] presents a partial reflective ground plane-based monopole suitable for 2.4GHz application which is also not so compact. A dual band antenna suitable for 2.4 and 60 GHz is presented by Sun et al. [5]. A single band circular polarized antenna based on two circular slots is presented by the authors in [6]. A flexible antenna based on two inverted U slots is presented in [7] which has extreme low thickness but with more surface area. A microstrip based single band antenna with a multilayer huge structure is discussed in [8].

Planar Inverted F single band Antenna having two stacked rectangular patch is discussed by the authors in [9]. In [10] a triple layer structure having a circular patch inside a rectangular loop patch with dual mode operation is discussed. An enhanced gain X shaped antenna structure is presented in [11] which is not compact at all. A complex structure based wearable antenna with a square patch inside a ring is discussed in [12].

A meta-material based defective ground single band antenna having dual planar structure is presented in [13]. In [14], a dual radiator-based antenna with J and L slots is presented which is very complicated structure. A 3D spiral structure is used for the effective reduction of size of antenna in [15] but which is not a planar one. Shorting Vias based compact antenna is presented in [16] which is very complicated in structure wise considerations.

In this article, we introducing an ultra-compact electrically small radiating structure operating at 2.4 GHz, which is found to be the most compact antenna ever discussed in literatures till now. Developed antenna found its applications on different areas such as ISM and wireless applications like WiFi 802.11b,802.11g, 802.11n, Bluetooth, ZigBee IEEE802.15.4 etc. Antenna offers uniform radiation characteristics within the band of operation with an apple shaped radiation pattern, very good radiation efficiency and with moderate gain. All these characteristics and compact size make this structure a very suited candidate for various wireless gadgets.

2. EVOLUTION OF ANTENNA

Evolution of the structure of compact radiator is depicted in Fig.1. It is developed from an extended ground nonconventional coplanar waveguide (CPW) fed structure having signal strip length less than ground plane length as shown in structure 1.

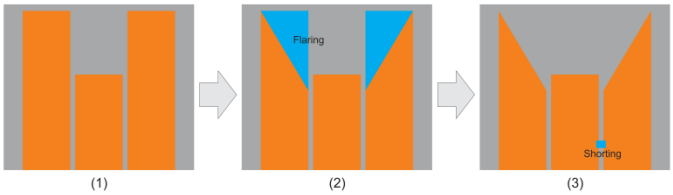

Fig.1. Evolution of the Compact Antenna

A flaring is introduced in both the ground planes by removing right angled triangular portions from each ground planes as shown in structure 2 of Fig.1. As the third step, a short is introduced in between one ground plane and signal strip which is our final antenna structure.

The simulated reflection co efficient (S_{11}) curves of all the three above structures are shown in Fig.2. From the Fig.it may be noted that for first two structures, there is no resonances but the introduction of the slot makes a resonant frequency near 2.4 GHz

Structure of the developed ultra-compact antenna with all the dimensional notations is given in Fig.3. Gap 'g' and signal strip width W_s of the structure are selected to meet 50Ω input impedance.

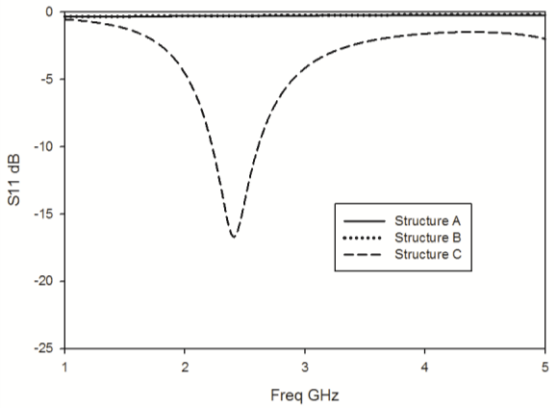

Fig.2. S_{11} of three structures shown in Fig.1

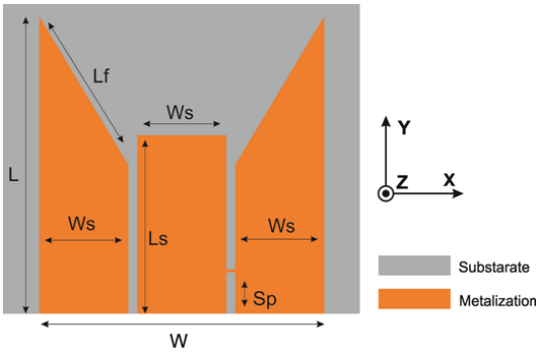

Fig.3. Structure with dimensional notations

3. PARAMETRIC OPTIMIZATION

To optimize the structure and to develop an application band-based prototype, a set of parametric analyses were performed with the help of ANSOFT HFSS software and the results obtained are discussed in this session.

As the first parametric variation, signal strip length Ls of the structure varied by keeping all other parameters constant. Result obtained is depicted in Fig.4. and it is found that the resonance gets lowered with increase in L_s. This is due to the increase in surface current path length with L_s.

The position of short is found to be very crucial in determining the resonance. The variation of S_{11} with short position S_p is given in Fig.5. It is found that the resonance gets a drastic up shift with increase in the parameter S_p.

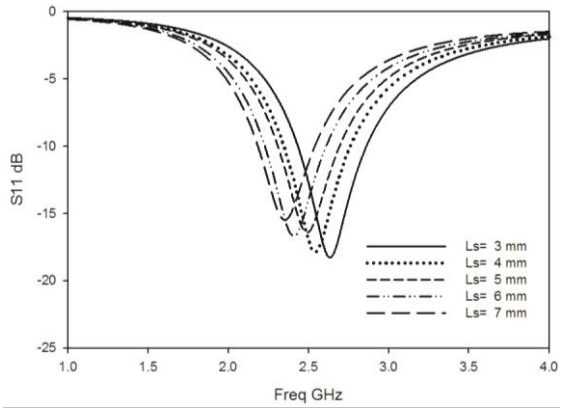

Fig.4. Effect of *Ls* on S_{11}

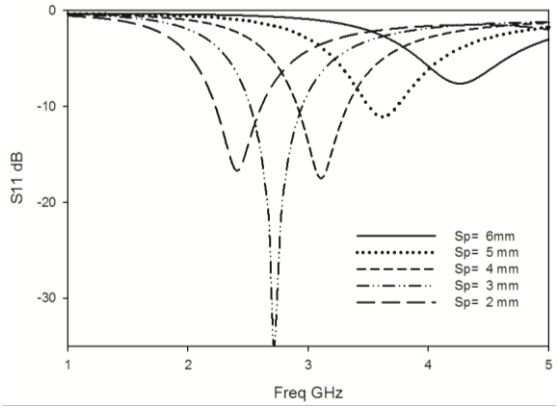

Fig.5. Effect of S_p on S_{11}

All other parameters like L, L_f widths of ground planes etc have minute effect on resonance and in all these cases, resonance remains unaltered with these parameters. Thus, it can be noted that the resonance determining factors in this structure are length of the signal strip and short position. From the parametric analysis, design equations of all the dimensions in terms of guided wavelength (λ_g) are developed and are detailed in Table.1.

Table.1. Parameters in terms of Guided Wavelength

Parameter	Design Equations
L	0.105163 λg
W	0.126195 λg
L_s	0.078872 λg
L_f	0.055736 λg
S_p	0.026291 λg

where λ_g corresponding to the guided wavelength corresponding to resonance and is calculated from free space wavelength λ using the expression:

$$\lambda_g = \frac{\lambda}{\sqrt{\varepsilon_{eff}}} \quad (1)$$

where ε_{eff} is the effective dielectric constant and is calculated from dielectric constant ε_r of the substrate using the equation

$$\varepsilon_{eff} = (\varepsilon_r+1)/2 \quad (2)$$

To validate these design equations, three different antennas in different substrates are designed and simulated. All the antennas are found to be resonates at a frequency which is placed closely to designed frequency. Parameters of the antenna designed using the developed equations and the results obtained are given in Table.2 and from the last two rows, it is evident that the design equations are universally valid for all kinds of substrates and all frequencies.

Table.2. Validation of Design Equations

Parameters	Antenna A	Antenna B	Antenna C
ε_r	2.2	4.4	10.2
L (mm)	4.79	8	7.4
W (mm)	5.75	9.6	8.88
L_s (mm)	3.59	6	5.55

L_f (mm)	2.54	4.24	3.92
S_p (mm)	1.19	2	1.85
Designed Freq (GHz)	5.2	2.4	1.8
Resonates at (GHz)	5.194	2.4058	1.806

4. RESULTS AND DISCUSSIONS

From the validation process of the antenna design equations performed, one antenna resonating at 2.4 GHz (Antenna B) is selected for making the prototype and for experimental studies and measurements. The structural specification of the antenna are depicted in table 3. Overall volume of the antenna is found to be $8 \times 9.6 \times 1.6$ mm^3 ($0.12\lambda g \times 0.10\lambda g \times 0.02\lambda g$) which makes the structure most compact one and entitled to the category of an electrically small antenna.

Table.3. Optimized dimensions of the structure

L	***W***	L_s	W_s	L_f
8 mm	9.6 mm	6 mm	3 mm	4.24mm
Sp	***g***	***h***	**tan δ**	ε
2 mm	0.3 mm	1.6 mm	.002	4.4

Simulated and measured S parameter of the antenna were in good agreement and is shown in Fig.6. The 2:1 VSWR bandwidth of the antenna ranges from 2.2 to 2.7 GHz (Bandwidth of 500 MHz) which is wide enough to cover Wi-Fi 802.11b,802.11g, 802.11n, Bluetooth, ZigBee IEEE802.15.4 and ISM application.

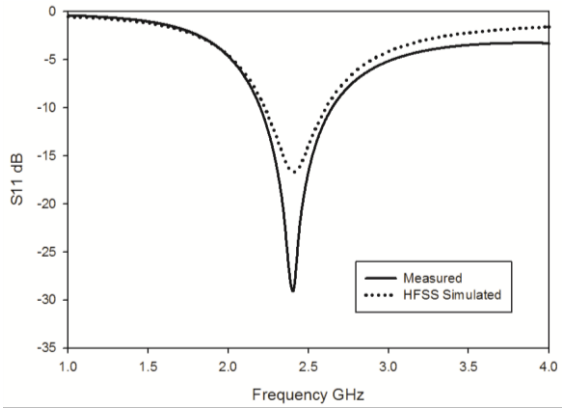

Fig.6. Measured and Simulated S_{11}

Two-dimensional energy distribution of the antenna around the structure in two principal planes are given in Fig.7. Polarization of the antenna is found to be linear with high degree of cross polar purity in both E and H plane.

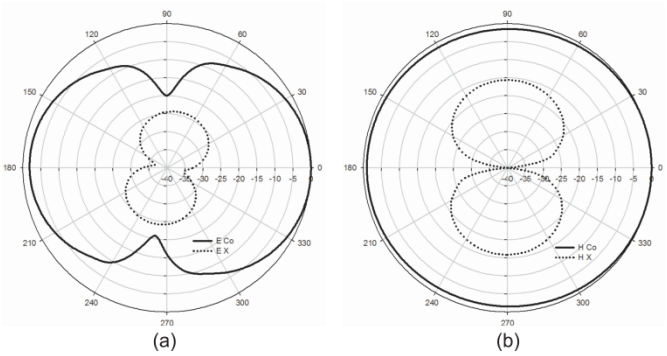

Fig.7. Measured Radiation Patterns (a) E plane and (b) H plane

Simulated 3D pattern of the antenna at 2.4GHz, obtained from ANSOFT HFSS is depicted in Fig.8. Antenna offers an apple shaped radiation pattern similar to a half wave dipole at resonance.

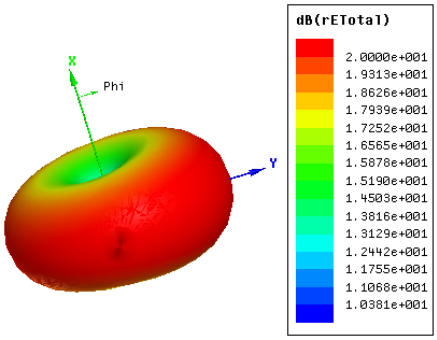

Fig.8. 3D Radiation Pattern

To obtain the technical knowhow of radiation mechanism, the surface current plot of the antenna is analysed thoroughly. The vector surface current plot of the antenna is given in Fig.9. Entire metallic surface contributes to radiation in this structure. One important factor to be noted in this structure is that the direction changes of surface current in right and left ground plane. In normal CPWs all the ground plane currents are in same direction. This directional change is due to the presence of the short in between signal strip and right ground plane. Current in signal strip also forcefully changes its current direction due to the short. As a result of these multiple folding in current path, current path length increases and which in turn results in lowering of the resonant frequency.

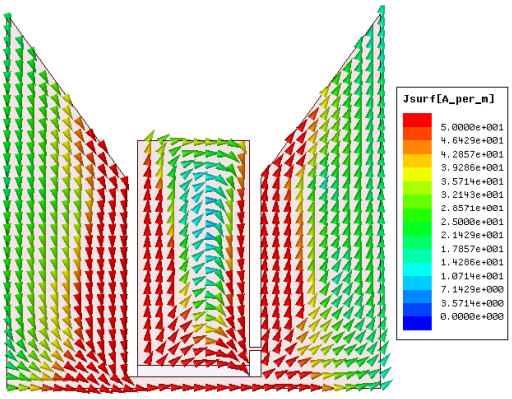

Fig.9. Vector Surface Current pattern

Wheeler cap method and Standard horn testing method are used to measure the radiation efficiency and gain of the antenna respectively.

The radiation efficiency is found to be 89% as its average value which shows the excellent and uniform radiation behaviour of the antenna in the entire band. The peak gain of the antenna is found as 2.65dBi around 2.39GHz with an average value of 2.6 dBi in the band. Both Efficiency and gain plot of the antenna are given in Fig.10.

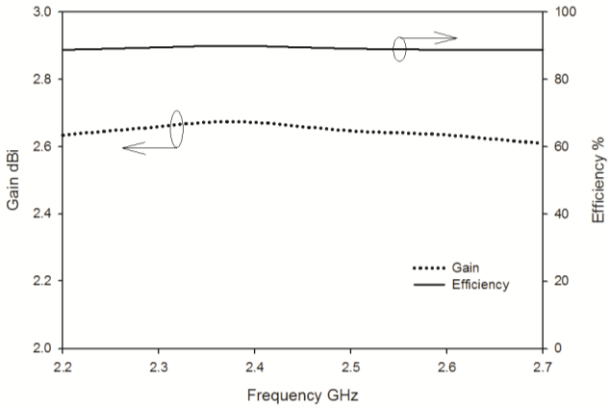

Fig.10. Efficiency and Gain plot

4.1 FDTD ANALYSIS

To unveil the mechanism behind radiation and other theoretical aspects about the CPW Fed Ultra Compact Radiator for 2.4GHz Wireless and ISM Applications, a mathematical model of the same is generated and simulated using FDTD method. The specification of Yee cell used in modelling are Δi=0.1mm, Δj=0.1mm and Δk=0.1mm. A total of 8000 repeated iterations are performed for better convergence with time step size Δt=0.5pS. FDTD computational domain with specified parameters are shown in Fig.11.

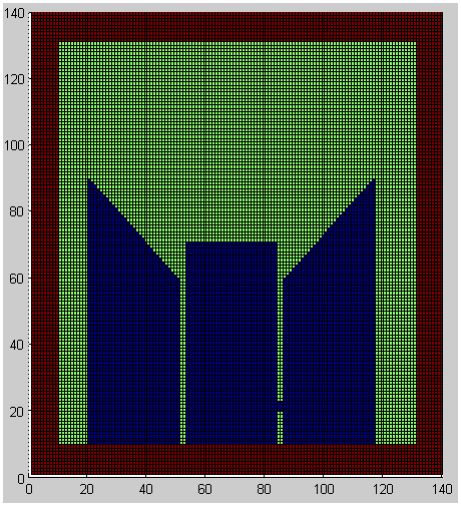

Fig.11. FDTD Computational Domain

For calculating the reflection characteristics in a wide frequency range, a narrow Gaussian pulse (Half power time period 10pS) is used as excitation. Time delay for excitation is selected as 90pS. A Perfectly Matched Layer (PML) absorption boundary condition explained in [17] is used as Absorbing Boundary Condition here.

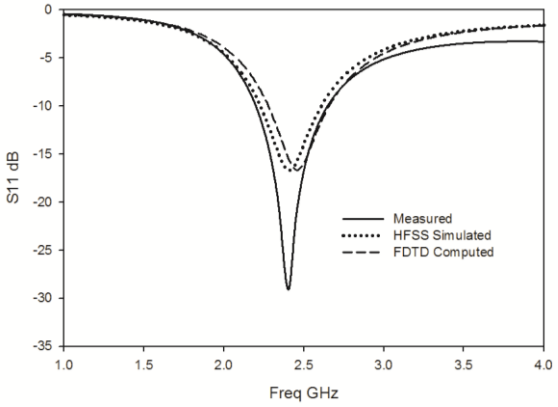

Fig.12. FDTD Computed and Measured S11

Measured, HFSS simulated and FDTD computed S11are found to be almost similar with excellent cross matching and can be verified from the Fig.12.

5. CONCLUSION

An ultra-compact uniplanar antenna suitable for 2.4GHz ISM and wireless applications like WiFi 802.11b,802.11g, 802.11n, Bluetooth, ZigBee IEEE802.15.4 etc. is developed and presented. Antenna offers uniform radiation characteristics within the band of operation with an apple shaped radiation pattern, very good radiation efficiency and with moderate gain. Universal design of the structure is developed and validated with the help of HFSS simulation software. FDTD modelling of the antenna is developed and results are compared with measured results.

REFERENCES

[1] S. Mekki, “Compact Single-Band Slot Antenna for WLAN Applications”, *Proceedings of IEEE International Workshop on Computer Aided Modeling and Design of Communication Links and Networks*, pp. 1-4, 2021.

[2] Hau Wah Lai and Kwai Man Luk, “Compact Dual-Band Antenna for IEEE 802.11ac”, *Proceedings of* European Conference on Antennas and Propagation, pp. 1-3, 2016.

[3] H. Kimouche and A. Mansoul, “A Compact Reconfigurable Single/Dual Band Antenna for Wireless Communications”, *Proceedings of European Conference on Antennas and Propagation*, pp. 393-396, 2011.

[4] M.V. Yadav and S. Baudha, “A Compact High Gain Partial Ground Plane Monopole Antenna for WLAN Application”, *Proceedings of International Conference on Information and Communication Technology*, pp. 1-4, 2018.

[5] Y.X. Sun, K.W. Leung and J.F. Mao, “Compact Dual-Frequency Antenna for 2.4/60 GHz Applications”, *Proceedings of Global Symposium on Millimeter-Waves*, pp. 100-102, 2017.

[6] T. Yo, C. Lee and C. Luo, “Small Single Band Circular Polarization and Dual Band Circular Patch Antenna”, *Proceedings of International Workshop on Antenna*

Technology: Small and Smart Antennas Metamaterials and Applications, pp. 435-438, 2007.

[7] A.B. Dey, B. Talukdar, S. Debnath and W. Arif, "Design of Flexible and Dual Wideband Antenna for Compact Wireless Devices", *Proceedings of IEEE International Conference on Advanced Networks and Telecommunications Systems*, pp. 1-6, 2019.

[8] W. Sadowski and C. Peixeiro, "Microstrip Patch Antenna for a GSM 1800 Base Station", *Proceedings of International Conference on Microwaves and Radar*, pp. 409-412, 1998.

[9] J. Barreiros, P. Cameirao and C. Peixeiro, "Microstrip Patch Antenna for GSM 1800 Handsets", *Proceedings of International Symposium on Antennas and Propagation Society*, pp. 2074-2077, 1999.

[10] V. Saideep and S.K. Behera, "Compact Dual-Mode Single-Band Microstrip Antenna for Body Area Network Applications", *Proceedings of International Conference on Wireless Communications, Signal Processing and Networking*, pp. 1-4, 2018.

[11] V.H. Mokal, S.R. Gagare and R.P. Labade, "Design of X-Shaped Multi Band Printed Antenna for GSM-1800, Bluetooth, Wi-MAX and WLANApplications with Improved Gain", *Proceedings of International Conference on Advances in Communication and Computing Technology*, pp. 12-17, 2018.

[12] C. Mendes and C. Peixeiro, "A Dual-Mode Single-Band Wearable Microstrip Antenna for Body Area Networks", *IEEE Antennas and Wireless Propagation Letters*, Vol. 16, pp. 3055-3058, 2017.

[13] K.K.A. Devi, N.C. Hau, C.K. Chakrabarty and N.M. Din, "Design of Patch Antenna using Metamaterial at GSM 1800 for RF Energy Scavenging", *Proceedings of IEEE Asia Pacific Conference on Wireless and Mobile*, pp. 157-161, 2014.

[14] H.S. Singh, K. Singh and R.M. Shubair, "A Compact Mobile Handsets MIMO/Diversity Antenna for GSM1800 and WiMAX Applications", *Proceedings of International Conference on Electrical and Computing Technologies and Applications*, pp. 1-4, 2017.

[15] J.L. Buckley, K.G. McCarthy, L. Loizou, B. O'Flynn and C. O'Mathuna, "A Dual-ISM-Band Antenna of Small Size using a Spiral Structure with Parasitic Element", *IEEE Antennas and Wireless Propagation Letters*, Vol. 15, pp. 630-633, 2016.

[16] N. Abbas, "A Compact Wide Band Implantable Antenna for Biotelemetry", *Proceedings of International Conference on Latest trends in Electrical Engineering and Computing Technologies*, pp. 1-5, 2019.

[17] J.P. Berenger, "A Perfectly Matched Layer for Absorption of EM Wave", *Computational Physics*, Vol 114, pp. 185-200, 1994.

COMPACT COPLANAR STRIP FED UWB ANTENNA WITH ENHANCED GAIN

Abstract

A coplanar strip fed enhanced gain directional radiator with a V shaped slot suitable for FCC specified ultra wide band application is developed. The 2:1 VSWR bandwidth of the antenna is nearly 9GHz ranging from 3.1 to 12 GHz. Proposed structure possess average radiation efficiency greater than 90% and a larger gain of 5 dBi in the entire range of frequencies of operation. Radiation patterns and polarization characteristics of the antenna are also uniform in entire band. Measured group delay of the structure is very minute and thus antenna has an excellent time domain performance. Transmitted and received pulses by the antenna are almost similar and thus the dispersion will be minimum.

Authors

Sreejith M. Nair[1], Manju Abraham[2], S. Sindhu[3], M.S. Nishamol[4]

Government College, Chittur, India[1], Baseliose Poulose II Catholicose College, India[2], Government College, Chittur, India[3,4]

Keywords

FULL TEXT PDF

Published By :
ICTACT

Published In :
ICTACT Journal on Microelectronics (Volume: 8 , Issue: 4 , Pages: 1437 - 1441)

Date of Publication :
January 2023

DOI :
10.21917/ijme.2023.0247

REJI T
2024.05.02 14:46:35 +05'30'